# WILDFIRE INFLUENCE ON RAINFALL CHEMISTRY AND DEPOSITION IN TEXAS DURING THE 2011-2014 DROUGHT

Thomas Williamson

Thesis Prepared for the Degree of

MASTER OF SCIENCE

UNIVERSITY OF NORTH TEXAS

August 2021

APPROVED:

Alexandra Ponette-González, Committee Chair
Lu Liang, Committee Member
Reid Ferring, Committee Member
Michael Olson, Committee Member
Steve Wolverton, Chair of the Department of Geography and the Environment
Tamara L. Brown, Executive Dean of the College of Liberal Arts and Social Sciences
Victor Prybutok, Dean of the Toulouse Graduate School

Williamson, Thomas. *Wildfire Influence on Rainfall Chemistry and Deposition in Texas during the 2011-2014 Drought*. Master of Science (Geography), August 2021, 53 pp., 7 tables, 10 figures, references, 69 titles.

From 2011 to 2014, one of the most severe and intense droughts in Texas recorded history led to widespread wildfires across the state, with unknown effects on atmospheric nutrient and pollutant deposition. The objectives of this research were to: (1) characterize the frequency, magnitude, and spatiotemporal distribution of Texas wildfires (2011-2014); (2) identify smoke occurrence and source regions at eight Texas National Atmospheric Deposition Program (NADP) National Trends Network (NTN) sites (2011); and (3) quantify the influence of wildfire on weekly rainwater chemistry and deposition in 2011 at three NADP sites (Sonora, LBJ Grasslands, Attwater Prairie NWR). Data on large wildfires, smoke occurrence, and rainfall chemistry and deposition were coupled with principal component and back-trajectory analysis to address these objectives. Between 2011-2014, 72% of all wildfires occurred in 2011, accounting for 90% of the total area burned. In total, there were 17 extreme wildfires (i.e., in the 95th percentile of hectares burned), of which 11 occurred in 2011. Wildfire activity was concentrated in West Texas ecoregions and consumed primarily shrub/scrub and grassland/herbaceous land cover. Although West Texas experienced the most wildfires, smoke at the NADP locations in 2011, the "high-fire year," was more frequent in East Texas due to regional wind patterns transporting smoke from diverse source locations. In 2011, weeks with smoke-influenced rain events—defined as weeks in which the rainfall event air mass trajectory intersected a smoke polygon, at any time, for at least one hour in the 72-hours prior to rainfall at the NADP site—had higher concentrations of $Ca^{2+}$, $Mg^{2+}$, $K^{+}$, $NH4^{+}$, and $SO4^{2-}$ compared to background samples (not affected by smoke). At LBJ Grasslands, four smoke-influenced rain samples deposited >49% of annual wet deposition for all ions. Principal component analysis identified wildfire as a key

component contributing to the variance in the dataset. Taken together, these findings highlight the potential atmospheric and ecosystem impacts of future megadroughts and associated wildfires on smoke occurrence and fire-related deposition in the Southern Plains region.

ACKNOWLEDGEMENTS

I would like to thank all those who made this research and experience a reality. I would like to first thank the entire UNT Department of Geography and the Environment for always being willing to help and encouraging me throughout my time as a master's student. I would like to thank Dr. Steve Wolverton for the many lessons he taught me about how to succeed and thrive as a graduate student. I would like to thank Keshia Wilkins and Michelle Hurt for all the work they did behind the scenes to support graduate students before, during, and after the disruption of COVID. I would like to thank friends and family for the encouragement and support along the way, especially my mom, who has made immense sacrifices to aid my education, and Makayla, who has stood by my side and supported me through the ups and downs. I also thank the members of my committee, Dr. Reid Ferring, Dr. Lu Liang, Dr. Michael Olson, and Dr. Kathleen Weathers, for the support, ideas, feedback, help and advice they provided during this project. Finally, I would like to thank Dr. Alexandra Ponette-González for the tireless hours and immense effort she put into helping me become a better student, academic, and person during this journey. It would not have been possible without you, and I am beyond thankful to have your support as a mentor and friend.

TABLE OF CONTENTS

Page

LIST OF TABLES

Page

LIST OF FIGURES

Page

# CHAPTER 1

# WILDFIRE, SMOKE, PRECIPITATION CHEMISTRY, AND DEPOSITION

## Introduction

Over the entirety of the contiguous US, wildfire regimes are changing (Salguero et al. 2020). Geographic Area Coordination Center regions are utilized by many agencies to monitor and facilitate wildfire response. Over the period from 1984-2017, the Northwest and Southwest regions showed significant increases in wildfire frequency, average wildfire size, and total annual burned acreage (Salguero et al. 2020). The California and Great Basin regions showed positive trends in average burned area (average wildfire size), while the Eastern region exhibited no trends across the measured parameters (Salguero et al. 2020). Another study on wildfire trends across the western US from 1950-2019 found that the average burned area of wildfires in this region grew from ~486 ha in the 1950s to ~1,416 ha in the 2010s, nearly a threefold increase (Weber & Yadav 2020). The latter study did not find changes in fire severity, however. In the Great Plains region, large wildfires >400 ha have also increased in annual number from 33.6 in 1994 to 116.8 in 2014, with total burned areas increasing by over 400% (Donovan et al. 2017). These documented changes in fire regimes are in large part due to climate change (IPCC 2014; Balch et al. 2017; USGCRP 2018), but also relate to ecoregion characteristics. In this literature review, I focus on wildfire and smoke emissions, drought, and deposition to ecosystems in the Great Plains and Southern Great Plains ecoregion, as it is the focal area for this study.

## Changing Wildfire in the US and Southern Great Plains

In the Southern Great Plains, megafires (>40,500 ha) frequently occur in the broad ecotone between forests and grasslands west of the 98$^{th}$ meridian due to climate and vegetation characteristics. Wooded areas provide fuel and have high burn intensities, while grasses provide

additional fuel and are easily consumed once a fire ignites (Lindley et al. 2019). Moreover wet-dry cycles provide favorable conditions for large fires: wet periods promote vegetation growth and are followed by fire-prone drought periods. After the Dust Bowl of the 1930s, the Prairie States Forest Projects encouraged farmers and home owners to plant Eastern Red Cedar in windbreaks across the Great Plains. This led to the encroachment of Eastern Red Cedar (*Juniperus virginiana*) and other flammable woody species into grasslands and heightened wildfire intensity in the Southern Great Plains (Hoff et al. 2017). In the Cross Timbers of Oklahoma, for example, Eastern Red Cedar accounts for roughly 21% of canopy cover (as of 2016), which corresponds to a 38% increase in fuel load (Hoff et al. 2017). These estimates are reflective of the encroachment of Eastern Red Cedar since the 1950s, when Eastern Red Cedar accounted for <1% of basal and stem areas, increasing to 22% of basal and 15% of stem area by 2010 (DeSantis et al. 2011). Eastern Red Cedar is invasive and has spread to other areas of the Great Plains, including Texas and Kansas, potentially signaling a similar trend in the future (Hoff et al. 2017). Despite the long history of megafires in the Great Plains, ecoregions are highly resilient and recover back to pre-wildfire norms in relatively short time periods (i.e., 1-5 years in most cases) post wildfire (Donovan et al. 2020). In fact, Donovan et al. (2020) found that only the wooded areas of the northwestern Great Plains showed significant decreases in tree population post-fire.

In sum, the Great Plains region shows evidence of significant alterations in the frequency, magnitude, and area burned by wildfires in recent decades. These patterns provide a glimpse of potential future drought-driven wildfire regimes as climate change further affects temperature and precipitation anomalies in the Great Plains region.

## Climatic Forcing and Drought

Favorable meteorological and climatic conditions for drought and wildfire occur frequently in arid regions across the US, including the Southern Great Plains. These conditions include temperature anomalies and infrequent precipitation, as well as other conditions, most notably: a low relative humidity, low soil moisture, and high wind speeds (McGregor 2015; Lindley et al. 2019; Wang & Wang 2020). Lindley et al. (2019) found that megafires in the Southern Great Plains are partly attributable to low-level thermal ridges in combination with an area of high pressure over Kansas, strong upper-level winds, and humidity and temperature anomalies. The 2011 Texas wildfire season, one of the worst on record (Donovan et al. 2020; Wang & Wang 2020), showed similar meteorological and climatological conditions; a ridge of high pressure over the central Great Plains with anomalously higher temperatures leading to increased evaporation, decreased soil moisture, and low cloud cover (McGregor 2015). Another key contributor to wildfires in the Southern Great Plains is the timing of anomalously wet periods followed by significant droughts (Nielsen-Gammon 2011; McGregor 2015; Lindley et al. 2019; Wang & Wang 2020). Prior to the exceptional drought of 2011, which severely impacted Texas, Oklahoma, and New Mexico, Texas underwent the wettest ten to fifteen years in its climatic history (Nielsen-Gammon 2011; McGregor 2015). Wet periods result in fuel accumulation, which can be readily ignited and consumed during a drought period. The combination of these two factors can greatly influence seasonal wildfire patterns. One study has shown that antecedent fuel for the winter-spring months is most conducive for wildfire development, while drought and precipitation were most influential 3-5 months prior to the winter-spring months and one month prior the summer season for wildfire ignition (Wang & Wang 2020).

Climate modeling is often utilized to relate past and current climatic related events to future scenarios. Nielsen-Gammon et al. (2020) investigated the future water budget of Texas. The study indicates that by the end of this century, water supply will be further stressed by increased temperatures, more sporadic rainfall and greater extreme rainfall events, further depleting soil moisture and increasing evaporative demand in the lower atmosphere. Under future warming scenarios RCP 4.5 (intermediate) and RCP 8.5 (high emissions, worst-case scenario), Cook et al. (2015) showed that drying and drought risk will increase in the Southwestern US (Arizona, New Mexico, portions of west Texas) and Central Plains region, with drying more severe in the Southwest. Their study also showed a <12% chance of a megadrought occurring from 1850-2005 and a >80% chance of a multidecadal megadrought under the high emission scenario between 2050-2099. These studies also highlight the importance of anthropogenic forcing on climatic shifts and drought (IPCC 2014; Cook et al. 2015; Williams 2020). Williams et al. (2020) found that anthropogenic induced increases in temperature and humidity anomalies as well as alterations in precipitation patterns, can account for up to 47% of drought severity (Williams et al. 2020). In sum, it is imperative to understand the effects of changing drought and fire regimes, including the potential for megadroughts and megafires, as these will affect emissions to the atmosphere as well as the redistribution of nutrients and pollutants via atmospheric deposition.

## Wildfire and Smoke Emissions

Drought-driven wildfire not only impact the biosphere via the burning of land, but also emit smoke containing gases and particles into the atmosphere (Mallia et al. 2015; Hu et al. 2016; Hallar et al. 2017; McClure & Jaffe 2018). When biomass is burned during wildfires, particulate matter, potassium, and black carbon are emitted into the atmosphere (McClure and

Jaffe 2018). In fact, biomass burning is the dominant source of black carbon emissions globally (Bond et al. 2013). Previous research shows that concentrations of organic compounds, potassium, and calcium can increase by a factor of up to 13 in the first two days after a wildfire event (Myers-Pigg et al. 2016). Biomass burning is also responsible for up to half of all carbon monoxide emissions and as much as 20% of nitrogen oxides emitted into the atmosphere from 1970-2000 (Olivier et al. 2005). Other studies have looked at trace gases and aerosols related to biomass burning, including carbon dioxide (Le Quéré et al. 2018), methane, nitrous oxide (Tian et al. 2016) and ammonia and sulfur dioxide (Ubranski 2014). Some of these gases contribute to increasing global temperatures, which, in turn, have a significant impact on drought occurrence, longevity, and severity, and thus wildfire occurrence (IPCC 2014).

Recently, a study conducted by Webster et al. (2016) looked at mercury emissions from wildfires in the western US finding that wooded forests produced the largest mercury emissions, while desert scrub produced significantly less in accordance with typical temperatures reached by these wildfires (Webster et al. 2016). Other research in the western US has found that roughly 24.2% of atmospheric $PM_{2.5}$ concentration are the result of nearby wildfire occurrences (Dadashazar et al. 2018). Yet another analysis on tropical regions looked at various ecoregions across Mexico, Central and South America, Africa, and Southeast Asia (Shi et al. 2020). This study looked at emissions from savanna/grasslands in the Americas, woody savanna/shrubland in Africa, and tropical forest in Southeast Asia. Results showed significantly higher emissions from tropical countries from 2011-2017, with emissions such as carbon dioxide occurring in woody savanna/shrubland accounting for 52% of all emissions, followed by savanna/grasslands at 27%, also noting that Africa contributed over threefold more emissions that the other regions.

In summation, emissions related to biomass burning are frequently studied. These

emissions can impact air quality by injecting large amounts of $PM_{2.5}$, carbon monoxide, and can lead to ozone formation. Some recent studies have investigated the patterns of increasing emissions from wildfires and what impacts that they might have on humans as well as affected ecosystems. Lastly, these emissions are typically not spatially bound and can travel long distances once injected into the atmosphere.

Indeed, smoke plumes can travel hundreds and thousands of kilometers in the atmosphere. These changes in air quality resulting from smoke emissions affect the chemical composition of rainwater because gases and particles can dissolve in water droplets within clouds or can become incorporated into water droplets as precipitation falls through the atmosphere. The process whereby these gases and particles are deposited to the surface in precipitation is referred to as wet deposition (Ponette-González et al. 2016).

## Wildfire-Related Deposition to Ecosystems

To date, few studies have quantified the influence of wildfire on the chemical composition of rainwater and deposition. However, those that have indicate that significant proportions (>30% in some cases) of nitrogen, phosphorus, and sulfur can be deposited in throughfall post-wildfire (Ponette-Gonzalez et al. 2016). Finally, research has shown that significant proportions of sulfur, potassium, zinc, and equivalent black carbon were deposited into Central Amazonia via the transport of smoke and wildfire emissions occurring elsewhere in the Amazon Basin – particularly in the dry season (Pauliquevis et al. 2012).

For instance, in some tropical forest peatlands in Southeast Asia, it has been shown that wildfire can strongly influence the total deposition to ecosystems despite accounting for a relatively low proportion of samples (Ponette-González et al. 2016). This study showed that > 30% of inorganic N and P, as well as ~20% of S flux was deposited after local and regional

wildfires (Ponette-González et al. 2016). As previously mentioned, nitrogen oxides and ammonia are prevalent emissions within tropical wildfires. It has been noted that elevated nitrate, ammonium, and phosphate deposition during a burning period from 1997-2006 occurred in this same region compared with non-biomass burning periods (Sundarambal et al. 2010). A similar study conducted in Sao Paulo State, Brazil, examined annual deposition fluxes during sugar cane burn-off. Results indicated fluxes as high as 44.3% for ammonium, 42.1% for potassium, 31.8% for magnesium, 5.2% for calcium, 3.8% for sulfate, and 2.3% for nitrate (da Roacha et al. 2005). Biomass burning has also been shown to be a significant source of phosphorus to tropical forests, such as the Amazon (Mahowald et al. 2005). Phosphorus deposition in the Amazon directly related to biomass burning accounts for roughly 23% of the overall flux in the region (Mahowald et al. 2005). Interestingly, the study by Mahowald et al. (2005) found that there is a net loss of phosphorus to the Amazon Basin due to biomass burning; concluding that much of the phosphorus emitted during local biomass burning events are carried downwind and/or deposited into the neighboring oceans.

Another study looked at uncharacteristically high ammonium deposition in the boreal Fennoscandia region during 2006 (Karlsson et al. 2013). The study found that several large-scale biomass burning events had occurred in the deciduous forest regions of Eastern Europe with trajectory analysis showing the plumes tracked to the Fennoscandia region, most heavily to central Sweden (see Figure 2 Karlsson et al. 2013). The authors note elevated potassium and calcium concentrations recorded in the samples, with increased throughfall deposition of ammonium (Karlsson et al. 2013). Biomass burning has also been shown to produce significantly high ozone and carbon monoxide to the arctic, setting a record in 2006 (Stohl et al. 2007). The study notes that collected snow samples contained significant amounts of potassium, sulfate,

nitrate, and ammonium – all of which were sourced from biomass burning events in the temperate forests of Eastern Europe and supports the notion of high ammonium transport northward to the arctic and Fennoscandia regions (Stohl et al. 2007; Karlsson et al. 2013).

Mercury deposition has garnered attraction recently, as estimates show up to a fivefold increase in atmospheric mercury since the industrial revolution (De Simone et al. 2015), 8% of which is directly related to biomass burning (Friedli et al. 2009). Mercury is believed to be most prominently emitted via deforestation of the Amazon, wildfires in the African savanna, tropical wildfires in Southeast Asia and wildfires occurring within the boreal forest regions of North America (De Simone et al. 2015). It is estimated that 75% of these mercury emissions are deposited into the world's oceans and seas, with the North Atlantic containing the highest depositional flux and the North Pacific receiving the largest total deposition of mercury (De Simone et al. 2015). The Arctic was also shown to receive disproportionally higher deposition of mercury, likely due to the boreal forest burning within North America. Mercury is of importance due to its toxicity, especially methylmercury, which humans consume when eating fish (De Simone et al. 2015). One study recently conducted in the Canadian boreal forests suggest that from 2010-2015, biomass burning events resulted in a threefold to sevenfold increase in mercury emissions compared to anthropogenic sources, with much of the deposition occurring in provinces west of Ontario (Fraser et al. 2018). This study found that no more than 9% of the total annual mercury deposition was from Canadian biomass burning, but local contributions were as high as 80% during the burn season (Fraser et al. 2018).

In conclusion, there have been relatively few studies conducted which analyzed the deposition of elements and ions from wildfires to the environment. Many of the studies which have been done focused on the deposition of analytes such as ammonium, nitrate, and

phosphorus, specifically related to wildfires occurring in tropical rainforests. Recent research has begun to analyze deposition of toxic mercury to bodies of water as well as terrestrial ecosystems, as methylmercury is highly toxic to humans. Overall, the studies which have been conducted indicate significant annual proportions of deposition of nutrients to ecosystems are provided by wildfire.

## Conclusion

Wildfire trends across the Western, Southwestern, and Great Plains regions of the US have shown increased frequency and magnitude of wildfires in recent decades (IPCC 2014; Balch et al. 2017; Donovan et al. 2017; USGCRP 2018; Salguero et al. 2020; Weber & Yadav 2020). These wildfire increases are largely attributed to climatic and meteorological patterns conducive to drought and wildfire regimes (McGregor 2015; Lindley et al. 2019; Wang & Wang 2020) but are also aided by natural transitions in land covers such as grassland-woodland (Hoff et al. 2017; Lindley et al. 2019). Biomass burning can produce numerous particulate emissions into the atmosphere (Mallia et al. 2015; Hu et al. 2016; Hallar et al. 2017; McClure & Jaffe 2018) where they can be transported thousands of kilometers before being deposited to the environment via deposition. This biomass burning induced deposition has been shown to contribute considerable proportions of annual nutrients such as N, P, and S to the environment (Ponette-González et al. 2016), as well as other ions such as $Ca^{2+}$, $K^{+}$, and $Mg^{2+}$ (da Roacha et al. 2005). However, there is a substantial gap in the literature regarding the impact of wildfire on precipitation chemistry and deposition to the environment. As drought and wildfire regimes continue to alter amidst climate change, it is imperative to understand the impacts these regime changes will have to humans and the environment.

# CHAPTER 2

# WILDFIRE INFLUENCE ON RAINFALL CHEMISTRY AND DEPOSITION IN TEXAS DURING THE 2011-2014 DROUGHT

## Introduction

From 2011 to 2014, the State of Texas experienced a historic drought (Nielsen-Gammon 2011; McGregor 2015). The drought peaked in 2011, coinciding with the largest number of wildfires across the state for the whole of the drought period. Extreme droughts are also fueling major wildfire episodes in other areas of the US (Donovan et al. 2017; Hallar et al. 2017). The Western US, for instance, has experienced an addition of seven wildfire events annually since the 1980s as a result of increasing drought in the region (Dennison et al. 2014; Balch et al. 2016; Westerling 2016). Wildfire and severe drought are also increasing across the southwestern US (Cayan et al. 2010; Cook et al. 2015; Donovan et al. 2017), a region with land cover and ecoregion similar to those of West Texas. Meanwhile, the entirety of the Great Plains is experiencing more variable timing of precipitation and extremes in precipitation events (e.g., heavier rainfall; Prein et al. 2017). These changing drought regimes coupled with anomalous temperature and precipitation patterns have resulted in an increase in the frequency, intensity, and geographic distribution of wildfire, with new and continuing impacts across social, economic, and environmental realms (USGCRP 2018).

Wildfires can affect various aspects of the environment, including air quality, as large plumes of smoke are injected into the atmosphere as fuel burns. For instance, when biomass is burned during wildfires, particulate matter, potassium, and black carbon are emitted into the atmosphere, reducing air quality (McClure and Jaffe 2018). These changes in air quality have the ability to affect the chemical composition of rainwater as gases and particles can dissolve in

water droplets within clouds or can become incorporated into water droplets as precipitation falls through the atmosphere. The process whereby these gases and particles are deposited to the surface in precipitation is referred to as wet deposition and can greatly impact ecosystems (Ponette-González et al. 2016).

Increasing aridity and variable precipitation patterns across the Great Plains and Texas are likely to lead to an increase in frequency, magnitude, and areas affected by wildfires in the future (IPCC 2014). These changes will ultimately affect atmospheric deposition rates and patterns. Yet, there is currently a lack of understanding of how wildfire affects the chemical composition of rainwater as well as nutrient and pollutant deposition to the environment. Therefore, in the context of this exceptional drought period, the objectives of this research were to: (1) characterize the frequency, magnitude, and spatiotemporal distribution of Texas wildfires during the 2011-2014 drought; (2) identify smoke occurrence and source regions at eight Texas National Atmospheric Deposition Program (NADP) National Trends Network (NTN) sites during 2011; and (3) quantify the influence of wildfire on weekly rainwater chemistry and deposition in 2011 at three NADP sites (Sonora, LBJ Grasslands, Attwater Prairie) (Figure 1).

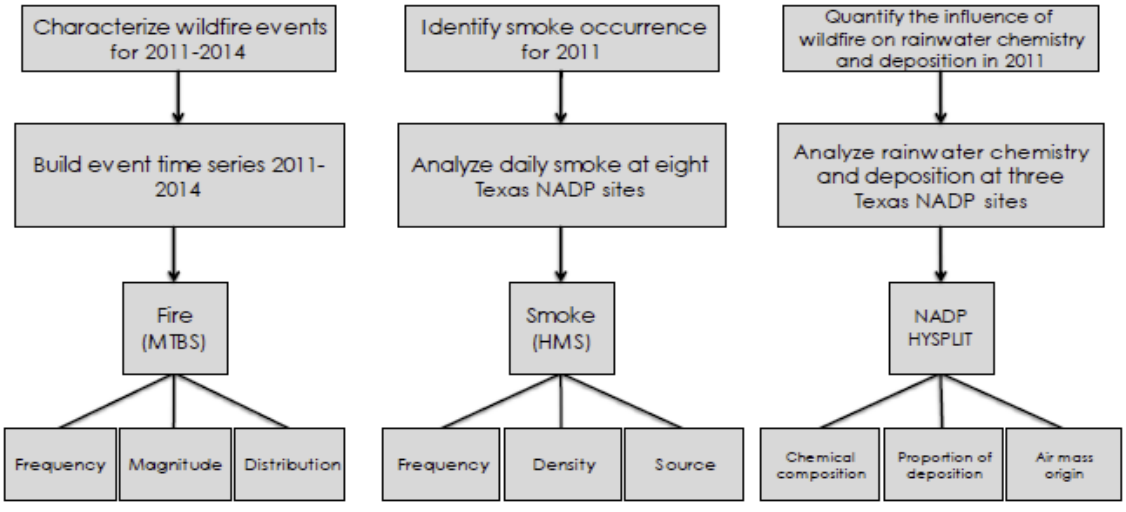


**Figure 1: Flowchart of research objectives (top row), approach to accomplish each objective, and datasets used.**

## Background and Methods

### The 2011-2014 Drought

Beginning in fall of 2010 and extending through fall and into winter of 2014, a severe drought occurred in the South, Southeast, Midwest and Ohio Valley regions of the US. The onset of the drought coincided with a La Niña event that formed in the tropical Pacific Ocean (Hoerling et al. 2013). La Niña events tend to shift storm tracks of west-approaching and western storms into a more northerly direction. This results in downwind effects, creating the potential for reduced rainfall and drought in much of the Midwest and Southern US (Seager et al. 2014). However, La Niña alone did not produce what would become one of the most severe droughts in Texas history. During winter of 2010 and extending into spring of 2011, the North Atlantic Oscillation, another major driver of climatic patterns in the eastern US, shifted into a negative phase and caused a weakened pressure gradient over the north Atlantic. A weakened pressure gradient generates dry, polar continental air over Canada, which coupled with a weakened jet stream, allows the dry air to penetrate deeper into the eastern and southeastern US (Maidens et al. 2013).

Impacts of La Niña were immediately felt beginning in 2010 as Texas and Georgia recorded record lows in annual precipitation. Other southern states also recorded near record low precipitation. In 2011, the drought was primarily confined to the Southeast as several states experienced abnormal amounts of severe weather. As 2011 progressed, Texas had its second-driest year on record, Oklahoma had its fourth, and the drought began to expand through the winter. By spring of 2012, the drought had affected areas from the Southeast, Midwest, Great Plains, and Ohio Valley. The peak of the drought occurred in summer 2012, when nearly 81% of the continental US was under drought conditions. Texas had 25% of its area remaining in

extreme or exceptional drought by December 2012 (Ponette-González et al. 2018). By 2013, heavy rainfall and snowfall alleviated the drought in much of the affected region, but the Great Plains region did not receive relief until the latter half of 2014.

Precipitation differences across the State of Texas were vast during the drought. Areas of precipitation decreased in an east to west gradient, with East Texas receiving greater rainfall than West Texas during each year of the drought. In fact, in 2011, much of West Texas recorded <254 mm of precipitation, with areas nearer to Central Texas recording up to 508 mm. In contrast, East Texas received ~508 to ~1,000 mm. In 2012, much of West Texas received up to 508 mm, while East Texas precipitation increased to ≤1,270 mm. As 2013 ended, West Texas recorded ≤635 mm, with some areas receiving closer to 700 mm, while East Texas remained in the ≤1,270 mm range. By the end of 2014, nearly all of West Texas received ~508 mm of precipitation while East Texas ranged from ~700 mm to as much as 1,270 mm (https://water.weather.gov/precip/download.php). These patterns illustrate the severity of the drought in 2011 as well as the contrasting annual precipitation received between West and East Texas.

## Characterization of 2011-2014 Texas Wildfires

The frequency, magnitude (area burned (ha)), and spatiotemporal distribution of Texas wildfires were examined for the entirety of the 2011-2014 drought. To analyze these wildfire attributes, the Monitoring Trends in Burn Severity (MTBS) dataset was downloaded (https://www.mtbs.gov/direct-download) for the State of Texas for each year in the focal period.

This database maps the burn severity and extent of US wildfires which are >405 ha in the Western US or >202 ha in the Eastern US and combines this information with MODIS and Landsat imagery to produce GIS available files (MTBS 2020). This product has been used, for

example, to: develop classifications of tree mortality in the Pacific Northwest, investigate changes in fire regime in the Northern Rocky Mountains, and analyze land cover type burned during, and land cover type remaining after, fires in the Western US (Zhao et al. 2015; Whittier & Gray 2016; Shaw et al. 2017). Because of the resolution of MODIS imagery, MODIS products excel at tracking large fires. MTBS selectively archives only those wildfires which meet minimum burned area requirements and has the benefit of the Landsat database extending back to 1984 (MTBS 2019).

The frequency and magnitude of wildfires were determined utilizing their geographical coordinates and burned perimeter data supplied with the MTBS archives. Extreme wildfires were classified as those which fell within the 95$^{th}$ percentile of hectares burned. Descriptive statistics were used to characterize wildfires annually and over the entire focal period.

Identification of Smoke Occurrence and Source Regions

Analysis of smoke occurrence and source regions was conducted at eight National Atmospheric Deposition Program (NADP) National Trends Network (NTN) stations across the State of Texas (Figure 2). The National Atmospheric Deposition Program was founded in 1977 and provides data on spatial and temporal patterns of precipitation chemistry and deposition in the US (http://nadp.slh.wisc.edu/NADP/). As of 2020, there were 263 sites within the NADP NTN network.

In the State of Texas, NADP NTN sites span ~982 km: from the Guadalupe Mountains in West Texas to the Attwater Prairie Chicken National Wildlife Refuge in East Texas. Here we use the 100$^{th}$ meridian (100°W longitude) as the division between West and East Texas. The sites lie within seven ecoregions (Figure 2; https://tpwd.texas.gov/education/hunter-education/online-

course/wildlife-conservation/texas-ecoregions) and receive annual precipitation amounts ranging from ~300 mm to over 1000 mm (Table 1).

Big Bend National Park in the Chihuahuan Desert ecoregion is a semi-arid/arid area covered with desert scrub, grassland, yucca and juniper, and piñon pine and oak. Muleshoe National Wildlife Refuge is located ~105 km northwest of Lubbock in the Southern High Plains (Llano Estacado) ecoregion. Vegetation consists mainly of short prairie grasses, but large swaths of land have been converted to agriculture, which is their primary land use (https://tpwd.texas.gov/education/hunter-education/online-course/wildlife-conservation/texas-ecoregions). Cañónceta, also in the High Plains ecoregion, is dominated by short-grass prairie composed mostly of buffalo grass, but invasive mesquite has begun to spread across the region. Guadalupe Mountains National Park Frijole Ranger Station in far West Texas is also located in the Chihuahuan Desert ecoregion. Here, desert scrub, grassland, yucca, juniper, pinon pine and oak are dominant. Sonora, in the western part of the Edwards Plateau ecoregion, is characterized by grassland, juniper and oak woodlands, and plateau live oak or mesquite savannah vegetation. Beeville is located ~160 km south-southeast of San Antonio, Texas, within the East Central Texas Plains ecoregion. The area is dominated by taller brush in some areas, while hackberry and shorter brush are prevalent in others. Typically, grassland vegetation and semi-tropical species from Mexico can be found in the area. L.B.J. National Grasslands is located ~100 km north of the Dallas-Fort Worth metroplex in the Western Cross Timbers ecoregion. Vegetation in the area consists of high-density forested areas containing blackjack or post oak, with large amounts of prairie grasses including blue stem and buffalo grass. Attwater Prairie Chicken National Wildlife Refuge is located ~100 km west of Houston within the Western Gulf Coastal

Prairie. Primary land cover includes remnants of tallgrass prairies with oak parklands and oak mottes scattered across the area.

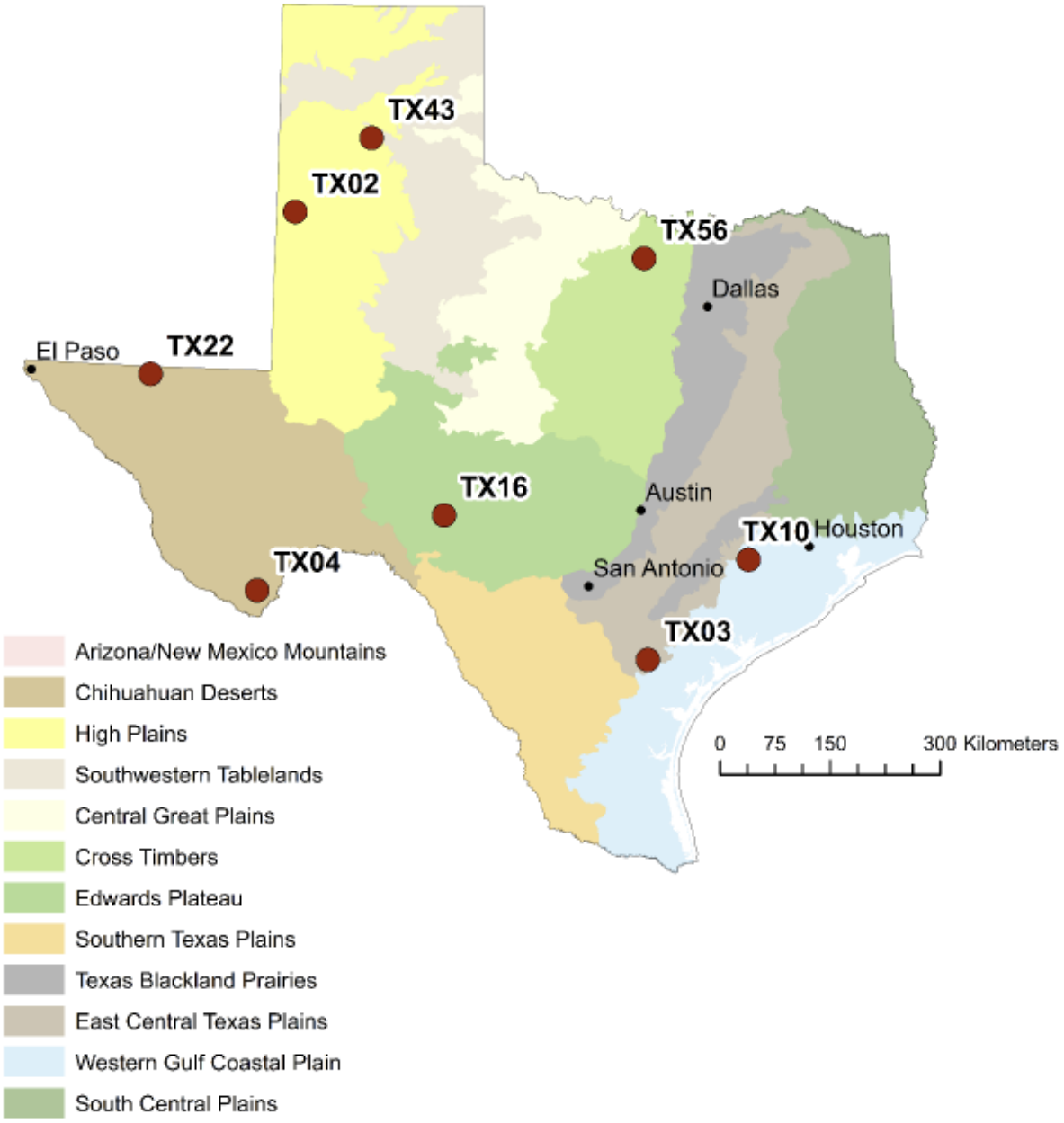


**Figure 2: State of Texas, United States, featuring each level 3 ecoregion within the state (U.S. Environmental Protection Agency. Corvallis, Oregon, 2021) and locations of National Atmospheric Deposition Program (NADP) sites (red circles).**

**Table 1: Descriptions of the Eight NADP NTN Sites within the State of Texas, Including Site ID, Latitude and Longitude, Mean Annual High and Low Temperature, Mean Annual Rainfall, Predominant Wind Direction, and Ecoregion. Sites are Organized from West to East.**

| Site ID | Name | Lat | Long | Annual High/Low (C)[a] | Mean Annual Rainfall (mm)[b] | Predominant Wind Dir[c] | Ecoregion |
|---|---|---|---|---|---|---|---|
| TX22 | Guadalupe Mountains National Park Frijole Ranger Station | 31.9069 | -104.805 | 27/7 | 494 | SSW | Chihuahuan Desert |
| TX04 | Big Bend National Park | 29.3025 | -103.1781 | 27/13 | 301 | NE | Chihuahuan Desert |
| TX02 | Muleshoe National Wildlife Refuge | 33.9557 | -102.776 | 23/4 | 434 | WSW | High Plains |
| TX43 | Cañónceta | 34.8800 | -101.665 | 22/6 | 471 | W | High Plains |
| TX16 | Sonora | 30.2613 | -100.5551 | 26/10 | 560 | S | Edwards Plateau |
| TX03 | Beeville | 28.4667 | -97.7069 | 27/16 | 760 | SE | East Central Texas Plains |
| TX56 | L.B.J. National Grasslands | 33.3917 | -97.6397 | 24/10 | 863 | SSE | Western Cross Timbers |
| TX10 | Attwater Prairie Chicken NWR | 29.6614 | -96.2594 | 27/14 | 1024 | SSE | Western Gulf Coastal Plain |

[a]Temperature from National Climate Data Center (NCDC) (https://www.ncdc.noaa.gov/cdo-web/search). [b]Precipitation from NADP (http://nadp.slh.wisc.edu/data/sites/list/?net=NTN). [c]Wind direction from Iowa Mesonet (https://mesonet.agron.iastate.edu/plotting/auto/).

NOAA's Hazard Mapping System (HMS) Fire and Smoke product was utilized to determine smoke occurrence across the eight NADP locations within Texas for the year 2011 when the drought was most severe. The HMS combines real-time polar and geostationary satellite imagery with expert image analysis. HMS has the benefit of utilizing numerous satellites (AVHRR, GOES, MODIS), allowing for daily archives of active fire detection and smoke information for 24-hour periods for the US, Canada, and Mexico (McNamara et al. 2000; Brey et al. 2017).

The HMS fire product tracks the location of ignition for wildfires which are detected by satellite and visually confirmed by an analyst. This results in an increase in the number of wildfires detected and included in the database, but also opens the database up to human error and bias (Brey et al. 2017). The HMS smoke product is based on visual classifications of smoke plumes via GOES-16 and GOES-17 ABI true-color imagery, which is limited to the sunlit portion of orbit (https://www.ospo.noaa.gov/Products/land/hms.html#about). The expert analyst draws a smoke polygon which is associated with each wildfire. Smoke density is indicated by the color of the smoke polygon: green represents thin density, yellow represents medium density, and red represents thick density. Since the smoke polygons are at daily resolution, hourly data for smoke presence are not available.

An overlay analysis was conducted to determine the frequency of smoke days (defined as a day when a smoke polygon intersected an NADP site) as well as the frequency of smoke days by density at each of the Texas NADP sites in 2011. Smoke origin was visually determined by examining where the smoke plume originated. Smoke source regions were based on the categorizations and scheme of Brey et al. (2018) (Figure 3), with one exception. Canadian provinces were grouped into a single "CAN" region due to a lack of overall smoke polygons

originating in Canada. In addition to the CAN assignment, a Central American, "CAM" region was defined to contain all Central American countries as well as Cuba.

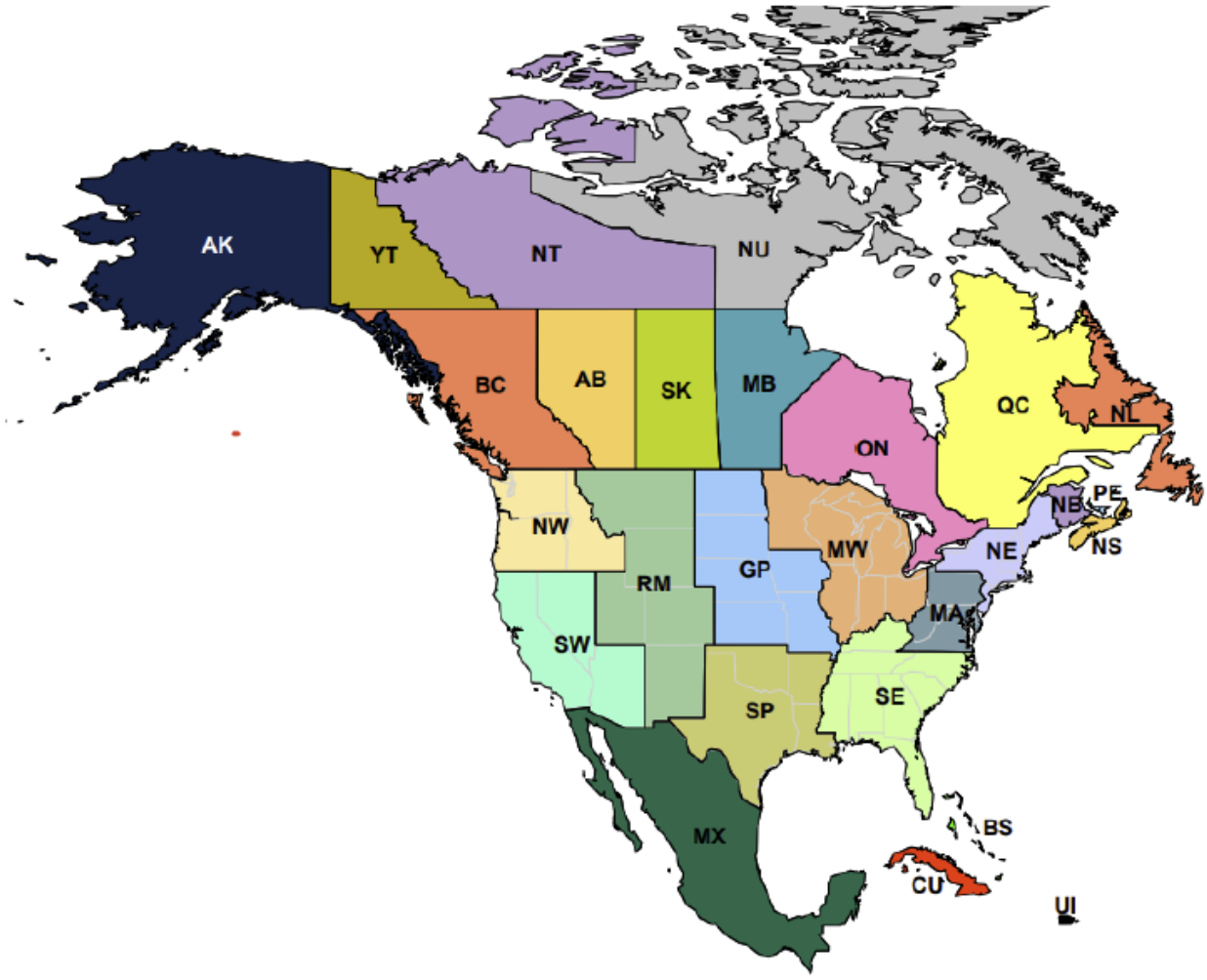


**Figure 3: Source and receptor regions per Brey et al. (2018); Northeast (NE), Mid Atlantic (MA), Southeast (SE), Midwest (MW), Southern Plains (SP), Great Plains (GP), Rocky Mountains (RM), Southwest (SW), Northwest (NW), Alaska (AK), US islands (UI), Mexico(MX), Quebec (QC), Nova Scotia (NS), Saskatchewan (SK), Alberta (AB), Newfoundland and Labrador (NL), British Columbia (BC), New Brunswick (NB), Prince Edward Island (PE), Yukon Territory (YT), Manitoba (MB), Ontario (ON), Nunavut (NU), Northwest Territories(NT), Cuba (CU), and Bahamas (BS), taken from Brey et al. (2018).**

Determination and Characterization of Smoke-Influenced Rain Events

The influence of wildfire on rainwater chemistry and deposition was investigated at three NADP sites (TX16, TX56, TX10) for the year 2011. To determine and characterize smoke-

influenced rain events, back-trajectories were computed for all rainfall events using NOAA's Hybrid Single-Particle Lagrangian Integrated Trajectory model (HYSPLIT v 5.0.0). HYSPLIT can be utilized to track a particle, or particles, backwards in time from a specific location. HYSPLIT was coupled with Eta Data Assimilation System (EDAS) meteorological data as it is the most utilized dataset for North American applications of HYSPLIT (https://webspace.clarkson.edu/projects/TraPSA/public_html/en/downloaddata.html).

For this study, backwards trajectories were run: (1) from three starting locations—NADP sites TX10, TX16, and TX56; (2) for 72-hours, and (3) at three heights: 500 m above ground level (agl), 1000 m agl, and 1500 m agl. Trajectories were then overlain onto the HMS smoke polygons to assess if the rainfall event air mass trajectory coincided with a smoke polygon. We define a smoke-influenced rain event as one in which the rainfall event air mass trajectory intersected a smoke polygon, at any time, for at least one hour in the 72-hours prior to rainfall being recorded at the NADP site. In addition, the total number of hours that the air mass trajectory intersected the smoke polygon was recorded for each model height. In cases where multiple trajectories were run in the same week (i.e., multiple rainfall events), hours of incidence for each height were summed together.

Analysis of Rainwater Concentration and Deposition

Volume-weighted mean (VWM) rainfall concentrations were calculated for background samples (weeks without smoke-influenced rain events) and smoke-influenced rain samples utilizing the formula:

$$\frac{\Sigma(Conc_i * Precip_i)}{\Sigma Precip_i}$$

where *i* represents the weekly sample data, *conc* is the solute concentration (mg/L), and *precip*

(mm) is the sample volume after adjusting for the collecting bucket surface area (678.9 $cm^2$). A nonparametric Wilcoxon signed rank test was then used to assess whether significant statistical differences existed between background and smoke-influenced rain samples. Significance was set at $p < 0.1$ and analyses were conducted in JMPv14.

Weekly wet deposition was calculated for all weeks using the formula:

$$WD = (Conc_i * Precip_i)$$

and reported in kilograms per hectare per week (kg/ha/week). Weekly wet deposition rates were then summed over the whole year for background samples and smoke-influenced rain samples. The proportion of annual wet deposition occurring during weeks affected by smoke-influenced rain events was calculated.

Air Mass Sources

To determine the prevailing air mass source regions, the Cluster Trajectory tool within HYSPLIT was utilized using the 1,000 m agl air mass trajectory for all rainfall events. This height was selected after examining smoke hours from each of the three heights. The 1,000 m agl height contained the most consistent smoke hours and the fewest days of no smoke presence. Furthermore, a 2010 study showed median plume heights for large North American wildfires to be roughly 850 m agl (Paugam et al. 2010).

The HYSPLIT Cluster Trajectory tool plots mean trajectories for a specified number of user-determined clusters. To determine the ideal number of clusters, a plot is created by the program which displays the total number of possible clusters (i.e., the total number of valid trajectories) on the x-axis and the total spatial variance amongst the potential clusters on the y-axis. There is no mathematical explanation for the 'correct' number of trajectories. Instead, the user must subjectively determine the number of clusters to be utilized, with the recommendation

to choose the value on the x-axis where the total spatial variance (TSV) spikes sharply upwards (https://www.ready.noaa.gov/hysplitusersguide/S255.htm).

Principal component analysis (PCA) was performed on the rainwater ion concentration data to identify associations among solutes (i.e., components) that can be interpreted in terms of sources (e.g., Hooper and Peters 1989). PCA was conducted for TX10, TX16, and TX56 in 2011. Before PCA could be run on the samples, data were log-transformed in R. After transforming the sample data, data were checked to ensure normality. In rare cases where the log transformation resulted in further skew or non-normality, original sample values were utilized. Data were standardized and all samples for the period were considered valid in accordance with NADP quality assurance/quality control standards and above detection limit.

To assess covariance and identify potential sources, PCA was performed on a linear correlation matrix of the NADP data for each site in 2011 – specifically utilizing the concentration values, site, and year. The components were then rotated utilizing a varimax rotation and the four strongest components reported.

## Results

### Spatiotemporal Distribution of Texas Wildfires (2011-2014)

During 2011-2014 historic drought, Texas experienced a large number of wildfires. In total, there were 324 wildfires that burned a total of 1,247,671 ha (Table 2). Spring and summer were the most active seasons for wildfires during the drought period (Figure 4).

The peak of the Texas drought occurred in 2011. During this year, 72% of all 2011-2014 Texas fires occurred during a fire season which spanned 350 days. Moreover, 11 of the 17 most extreme (95$^{th}$ percentile) wildfires occurred in 2011. These 2011 fires ranged from roughly 11,000 to ~121,000 ha. In 2012, the number of wildfires fell dramatically with no single month

producing more than five wildfires, and the length of the fire season also decreased. As drought conditions ameliorated in 2013, wildfires became more sporadic, and there was a reduction in the fire season length and the burned area. The 2014 fire season reflected improved drought conditions and contained the shortest fire season during the drought.

During the drought period, the majority of wildfires occurred in West Texas (Figure 5). Eastern, Central, and Southern Texas were impacted by fewer and smaller wildfires overall. West Texas ecoregions (High Plains, Southwestern Tablelands, Chihuahuan Desert) contained thirteen of the seventeen extreme wildfires. The dominant land cover types burned by the extreme wildfires were shrub/scrub (14 extreme wildfires (53-99%)) and evergreen forest (three extreme wildfires (42-68%)). The second dominant land cover burned was grassland/herbaceous, which accounted for eleven of the seventeen extreme wildfires. Shrub/scrub and evergreen forest constituted over 70% of all land cover burned for sixteen of the seventeen fires.

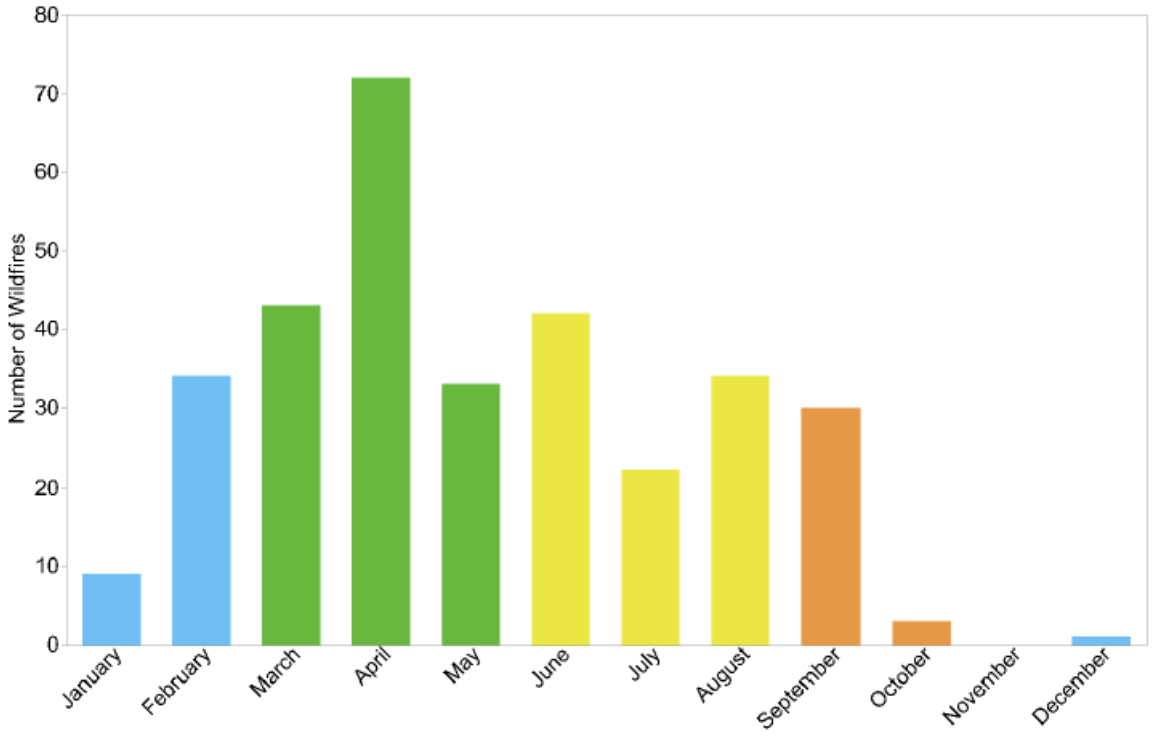


**Figure 4: Monthly distribution of wildfires across the State of Texas from 2011 to 2014. Bars are color coded by season; with winter – blue, spring – green, summer – yellow, fall – orange.**

**Table 2: Characteristics of Wildfires in the State of Texas, Including Burned Area (ha), Length of Fire Season (days), Number of Wildfires per Season, and 95th and 90th Percentile Fires (total ha burned) for Each Year from 2011 to 2014 and overall.**

| Year | Burned Area (ha) | Length (days) | Number of Fires | | | | | Percentile (total ha burned) | |
|---|---|---|---|---|---|---|---|---|---|
| | | | Spring | Summer | Fall | Winter | Total | 95th | 90th |
| 2011 | 1,123,540 (90%) | 350 | 90 (38%) | 83 (35%) | 29 (12%) | 32 (14%) | 234 | 693,464 | 766,654 |
| 2012 | 43,173 (4%) | 308 | 5 (22%) | 9 (39%) | 3 (13%) | 6 (26%) | 23 | 11,345 | 16,706 |
| 2013 | 28,409 (2%) | 259 | 20 (71%) | 2 (7%) | 1 (4%) | 5 (18%) | 28 | 3,962 | 5,702 |
| 2014 | 52,549 (4%) | 192 | 33 (85%) | 4 (10%) | 1 (3%) | 1 (3%) | 39 | 16,311 | 19,661 |
| 2011-2014 | 1,247,671 | 1,109 | 148 (46%) | 98 (30%) | 34 (11%) | 44 (14%) | 324 | 725,082 | 808,723 |

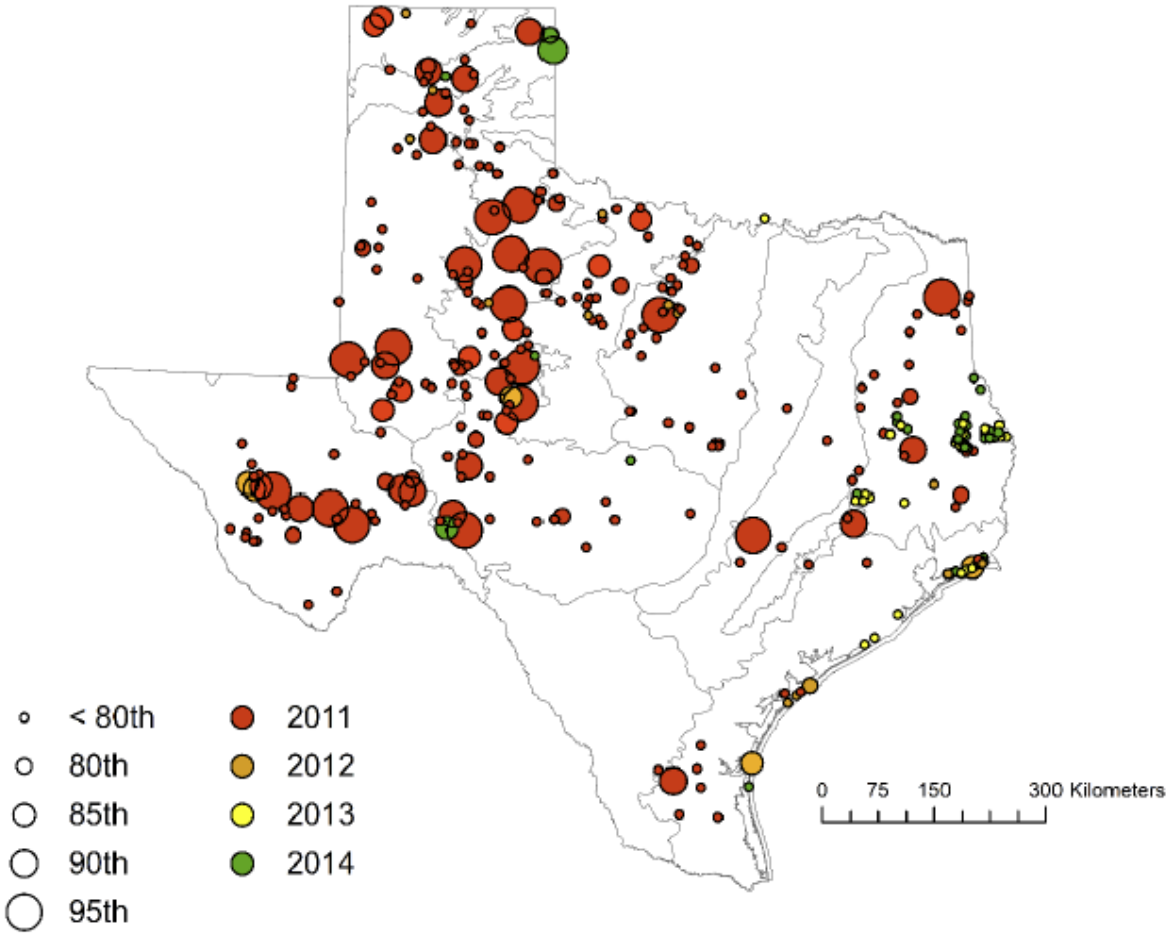


**Figure 5: Location of all wildfires during the 2011-2014 drought in the State of Texas. Dot size represents the percentile in terms of hectares burned, while dot color represents the year the wildfire occurred; red – 2011, orange – 2012, yellow – 2013, green – 2014.**

Smoke Occurrence and Source Regions

Smoke data revealed a clear separation in the number of smoke days among the NADP sites. With the exception of Sonora (TX16), which is located in West Texas, the East Texas sites had more smoke days compared to the West Texas sites (Figure 6). Smoke density followed a similar pattern. Excluding Sonora, the three East Texas sites had 45-65 light smoke days compared to 20-30 in the West Texas sites, 10-20 medium smoke days in the East compared to 5-15 in the West, and 3-7 high density smoke days in the East compared to 0-2 in the West.

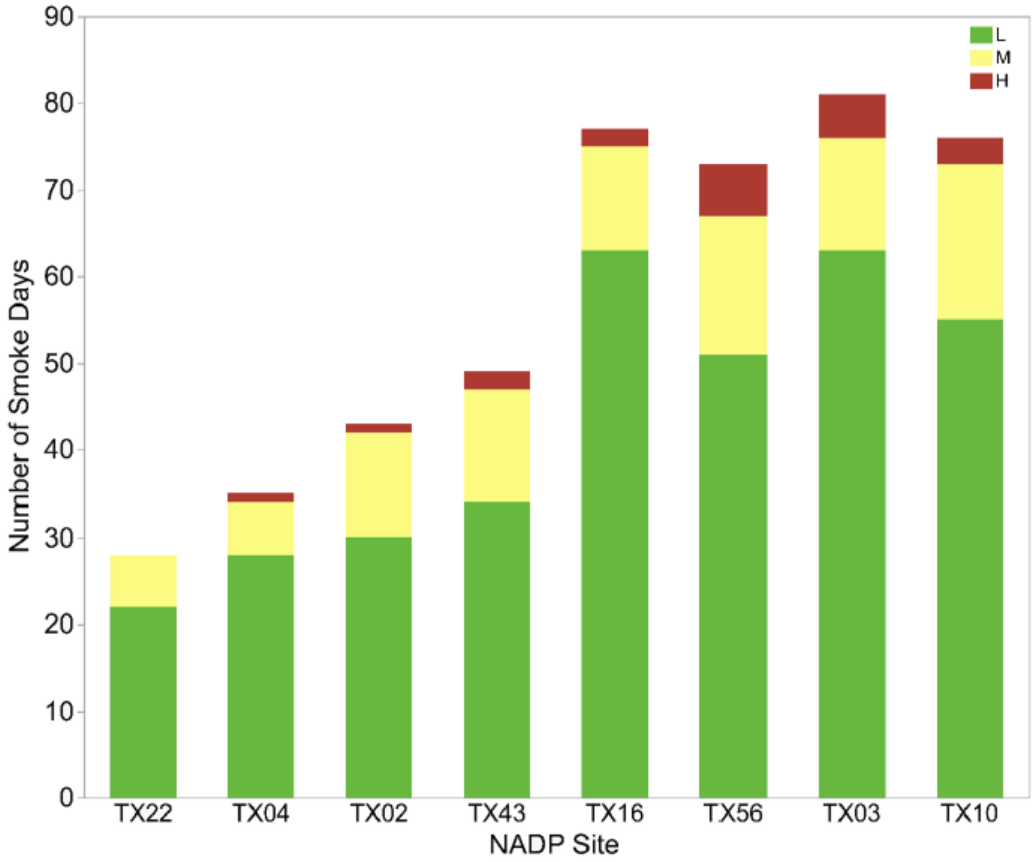


**Figure 6: Smoke occurrence (by smoke density category) at each of the Texas NADP NTN sites in 2011 during the historic drought period. Sites are organized from west to east. Green shading represents light (L) density smoke, yellow represents moderate (M) density, and red represents heavy (H) density smoke.**

Overall, the West Texas NADP locations were more prominently affected by the Rocky Mountain region, whereas the East Texas sites were more strongly affected by smoke from the Southern Plains region. The West Texas locations were affected by a more diverse and equally distributed source of smoke, while East Texas sites were more heavily dominated by a single region (i.e., the Southern Plains). The most prominent sources for smoke at Sonora were Mexico and the Southern Plains (Figure 7). Smoke was recorded from eight distinct regions at the LBJ National Grasslands site (Figure 7), with the Southern Plains contributing the most smoke days to the site. Smoke was recorded from seven distinct regions at Attwater Prairie Chicken NWR with the most prominent being the Southern Plains (Figure 7).


**Figure 7: The origin of smoke for eight Texas NADP NTN sites in 2011 during the historic drought period. Sites are organized from west to east. Color coding and region abbreviations mirror that of Brey et al. (2018), with the exception of Canadian provinces being combined into a single CAN grouping and the addition of a Central American, CAM region. MX represents Mexico; SW represents the Southwest; RM represents the Rocky Mountains; SP represents the Southern Plains; GP represents the Great Plains; SE represents the Southeast; and MA represents Mid-Atlantic.**

Rainwater Concentrations and Deposition

Volume-weighted mean rainfall concentrations revealed significant differences between background and smoke-influenced samples (Table 3). There were only two smoke-influenced rain samples at the Sonora site, however these samples had a nearly fourfold increase of $Na^+$ and $Cl^-$. The LBJ National Grasslands site showed significance amongst six analytes, including $Mg^{2+}$, $K^+$, and $Na^+$ ($p < 0.05$ level), as well as $SO_4^{2-}$, $Cl^-$, and $NH_4^+$ ($p < 0.1$ level). At Attwater Prairie Chicken NWR, $Ca^{2+}$ and $NH_4^+$ ($p < 0.05$), and $K^+$ and $NO_3^-$ ($p < 0.1$) were higher during smoke-influenced weeks compared to background sample weeks.

**Table 3: Volume-Weighted Mean Rainfall Ion Concentrations for Background and Smoke-Influenced Samples Collected at Three National Atmospheric Deposition Program Sites in Texas During the 2011 Drought - Sonora (TX16), LBJ National Grasslands (TX56), and Attwater Prairie Chicken NWR (TX10).**

| Dissolved Ion | Sonora | | LBJ National Grasslands | | Attwater Prairie | |
|---|---|---|---|---|---|---|
| | Background (*n* = 15) | Smoke-in-rain (*n* = 2) | Background (*n* = 14) | Smoke-in-rain (*n* = 4) | Background (*n* = 19) | Smoke-in-rain (*n* = 10) |
| | (mg/L ± SE) | (mg/L ± SE) | (mg/L ± SE) | (mg/L ± SE) | (mg/L ± SE) | (mg/L ± SE) |
| Calcium ($Ca^{2+}$) | 0.595 ± 0.186 | 0.382 ± 0.234 | 0.212 ± 0.056 | 0.503 ± 0.139** | 0.382 ± 0.234 | 1.806 ± 0.321 |
| Magnesium ($Mg^{2+}$) | 0.026 ± 0.016 | 0.035 ± 0.010 | 0.076 ± 0.02 | 0.083 ± 0.050 | 0.035 ± 0.010 | 0.110 ± 0.013** |
| Potassium ($K^{+}$) | 0.026 ± 0.011 | 0.031 ± 0.013 | 0.040 ± 0.007 | 0.063 ± 0.018* | 0.031 ± 0.013 | 0.146 ± 0.018** |
| Sodium ($Na^{+}$) | 0.126 ± 0.089 | 0.197 ± 0.024 | 0.576 ± 0.165 | 0.488 ± 0.412 | 0.197 ± 0.024 | 0.361 ± 0.034** |
| Sulfate ($SO_4^{2-}$) | 0.956 ± 0.198 | 0.933 ± 0.146 | 0.984 ± 0.131 | 1.397 ± 0.327 | 0.933 ± 0.146 | 1.720 ± 0.201* |
| Chloride ($Cl^{-}$) | 0.184 ± 0.118 | 0.313 ± 0.040 | 1.097 ± 0.339 | 0.847 ± 0.844 | 0.313 ± 0.040 | 0.550 ± 0.055* |
| Ammonium ($NH_4^{+}$) | 0.377 ± 0.070 | 0.357 ± 0.080 | 0.234 ± 0.032 | 0.483 ± 0.08** | 0.357 ± 0.080 | 0.991 ± 0.110* |
| Nitrate ($NO_3^{-}$) | 0.865 ± 0.195 | 0.820 ± 0.159 | 0.665 ± 0.097 | 1.360 ± 0.24* | 0.820 ± 0.159 | 1.628 ± 0.219 |

Note: SE = VWM standard error. *Significant at $p < 0.1$ level. **Significant at $p < 0.05$ level. ***Significant at $p < 0.01$ level.

**Table 4: Wet Dissolved Deposition for Background and Smoke-in-Rain Samples from Three National Atmospheric Deposition Program Locations in Texas During 2011 - Sonora (TX16), LBJ National Grasslands (TX56), and Attwater Prairie Chicken NWR (TX10). Wet Dissolved Deposition (WD) is Given in Kilograms per Hectare with the Overall Percentage of Total Deposition for each Ion Shown Next to the Deposition Amount.**

| Dissolved Ion | Sonora | | | | LBJ National Grasslands | | | | Attwater | | | |
|---|---|---|---|---|---|---|---|---|---|---|---|---|
| | Background (*n* = 15) | | Smoke-in-rain (*n* = 2) | | Background (*n* = 14) | | Smoke-in-rain (*n* = 4) | | Background (*n* = 19) | | Smoke-in-rain (*n* = 10) | |
| | WD Dep (kg/ha) | % Total | WD Dep (kg/ha) | % Total | WD Dep (kg/ha) | % Total | WD Dep (kg/ha) | % Total | WD Dep (kg/ha) | % Total | WD Dep (kg/ha) | % Total |
| Calcium ($Ca^{2+}$) | 1.90 | 92% | 0.15 | 8% | 1.48 | 29% | 3.65 | 71% | 0.96 | 72% | 0.38 | 28% |
| Magnesium ($Mg^{2+}$) | 0.08 | 83% | 0.02 | 17% | 0.13 | 38% | 0.22 | 62% | 0.35 | 85% | 0.07 | 15% |
| Potassium ($K^{+}$) | 0.08 | 85% | 0.01 | 15% | 0.12 | 29% | 0.29 | 71% | 0.18 | 80% | 0.05 | 20% |
| Sodium ($Na^{+}$) | 0.40 | 78% | 0.11 | 22% | 0.74 | 51% | 0.73 | 49% | 2.67 | 88% | 0.39 | 12% |
| Sulfate ($SO_4^{2-}$) | 3.18 | 93% | 0.22 | 7% | 3.55 | 51% | 3.48 | 49% | 4.41 | 81% | 1.07 | 19% |
| Chloride ($Cl^{-}$) | 0.59 | 77% | 0.17 | 23% | 1.18 | 52% | 1.11 | 48% | 5.08 | 89% | 0.67 | 11% |
| Ammonium ($NH_4^{+}$) | 1.25 | 91% | 0.11 | 9% | 1.36 | 41% | 2.00 | 59% | 1.05 | 75% | 0.36 | 25% |
| Nitrate ($NO_3^{-}$) | 2.90 | 91% | 0.26 | 9% | 3.14 | 49% | 3.29 | 51% | 2.99 | 75% | 1.00 | 25% |

The two smoke-influenced samples at Sonora resulted in 23% of $Cl^-$, 22% of $Na^+$, 17% of $Mg^{2+}$, and 15% of $K^+$ annual wet deposition (Figure 8). At the LBJ site, there were four smoke-influenced samples (22% of all samples), yet deposition ranged as high as 71% of the annual wet deposition for $Ca^{2+}$ and $K^+$, 62% for $Mg^{2+}$, 59% for $NH_4^+$, and 48-51% for all remaining analytes (Figure 8). At Attwater Prairie Chicken NWR, one-third of all rainwater samples were influenced by smoke to some extent (Table 3). Similar proportions of $Ca^{2+}$ (28%), $NH_4^+$ and $NO_3^-$ (25%) were deposited during these sample weeks (Table 4).

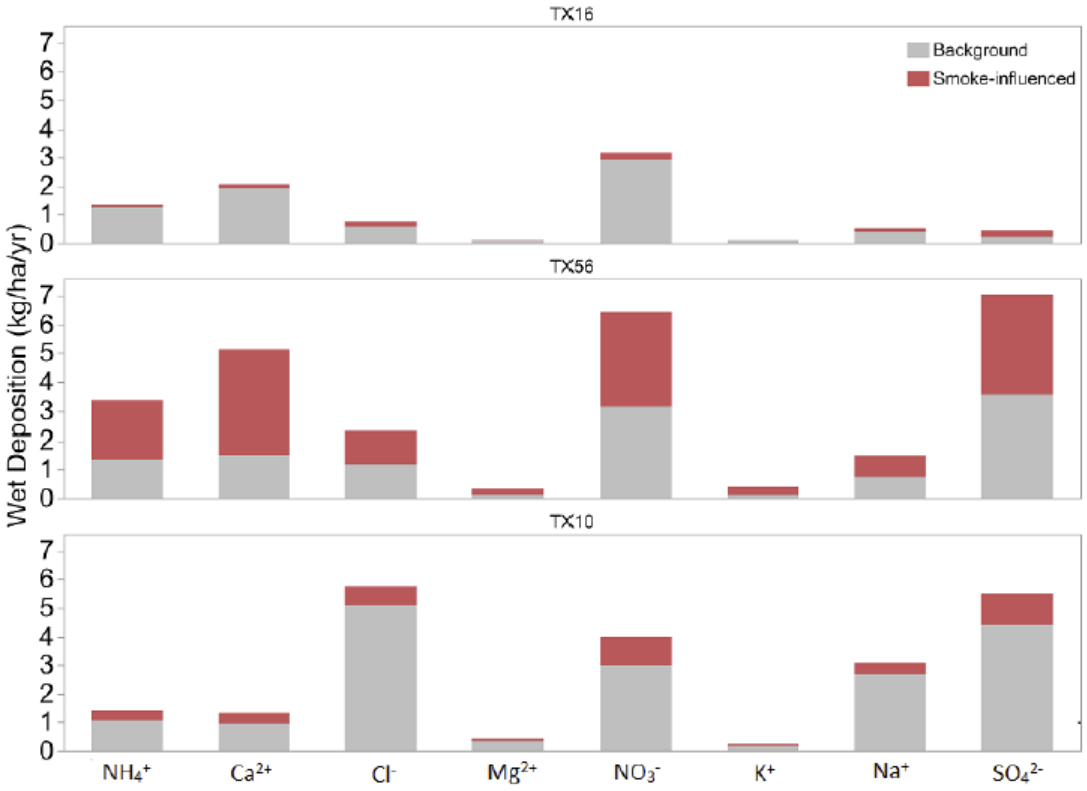


**Figure 8: Wet deposition for each analyte across three Texas NADP NTN sites for 2011 in kilograms per hectare per year. Gray represents background samples whereas red represents smoke-influenced rain samples. Sites are organized west to east (top to bottom), TX16 (Sonora), TX56 (LBJ National Grasslands), and TX10 (Attwater Prairie Chicken NWR).**

Air Mass Sources

At the Sonora site, 52% of trajectories were dominated by continental air masses (Figure 9). Approximately 43% of trajectories (cluster 3) show strong influence from major Texas

metropolitan areas such as Dallas-Fort Worth, Austin, and San Antonio. This site also had a strong influence from Gulf of Mexico sourced trajectories which represented a further 43% of the overall trajectories at the site (cluster 1). The remaining mean trajectories (clusters 2 and 4) were influenced by largely agricultural and shrub/scrub landcover in western Mexico (4%) and a pathway southeast along the Rocky Mountains of Utah, Colorado, and New Mexico (9%).

At the LBJ National Grasslands site, 51% of trajectories were dominated by oceanic air masses. Oklahoma City, Dallas-Fort Worth, Austin, and San Antonio metroplexes strongly influenced the mean trajectories (clusters 1 and 4) at LBJ. We note that at LBJ, 32% of all air masses tracked through the Great Plains and Midwest, while 17% of trajectories tracked through the desert Southwest.

At Attwater Prairie Chicken NWR, clusters one and three were primarily maritime, while cluster four was continental. Over land, the Attwater site showed strong influence from the Houston, Austin, and Dallas-Fort Worth metroplexes. The remaining trajectories reflected continental air masses from the Pacific Northwest and Great Plains, and Western Mexico. The Great Plains region is largely agricultural land, with small areas of shrub/scrub and grassland herbaceous landcover (https://www.usgs.gov/media/images/land-cover-conterminous-us-shown-16-thematic-classes). Western Mexico contains a mixture of agricultural and shrub/scrub land, with evergreen forested areas in the Sierra Madre Occidental and Oriental Mountain ranges (Pasos 2015).

At Sonora, there were four smoke-influenced trajectories (Figure 10). These trajectories originated from the Gulf of Mexico, Western Mexico, and the Rocky Mountains. The LBJ site also contained four smoke-influenced trajectories (Figure 10). Trajectories at this location originated from the Great Plains, Midwest, and Gulf of Mexico/Central America. The Attwater

Prairie Chicken NWR contained ten smoke influenced events which originated from the southeast (primarily maritime) and the northwest (continental).

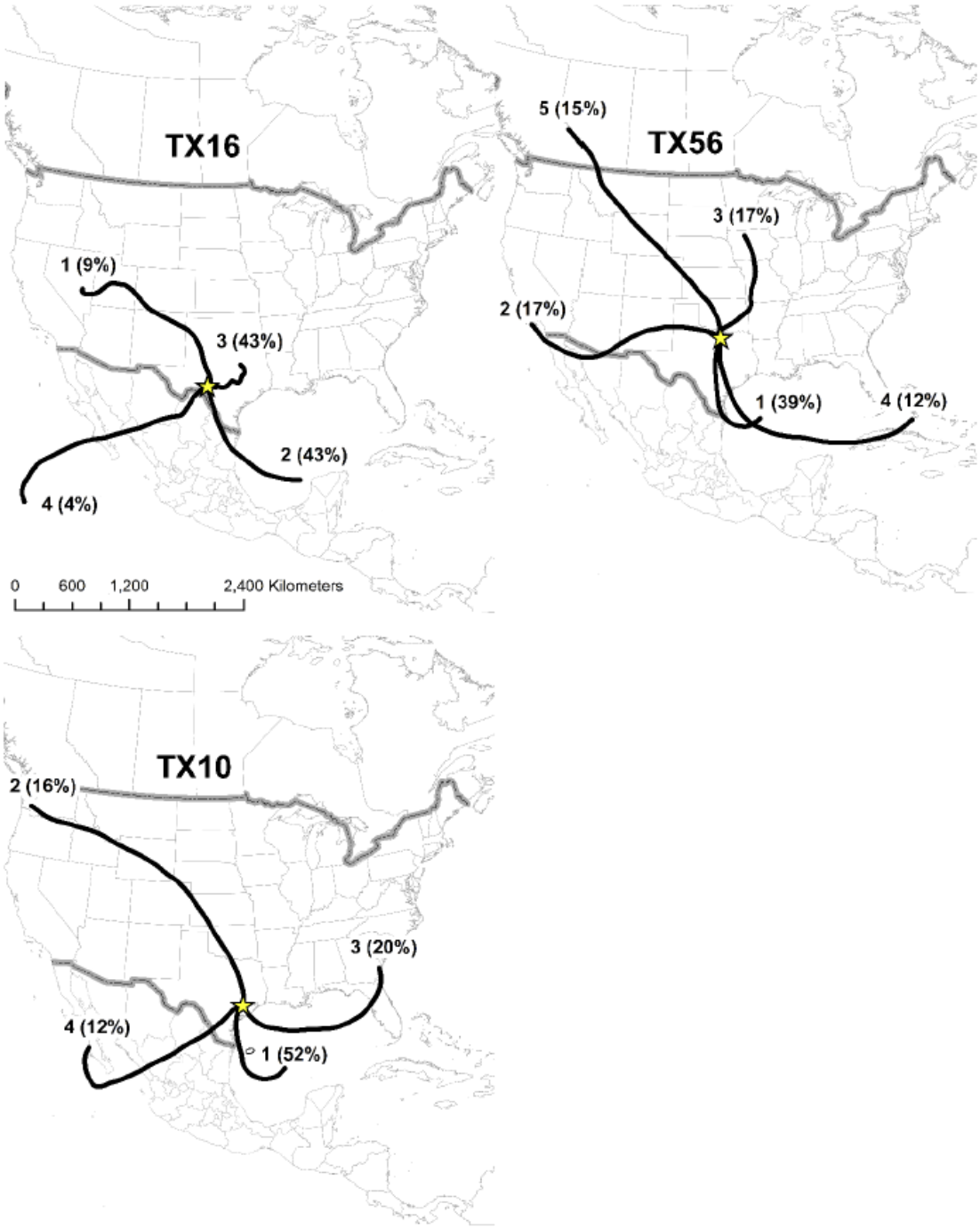


**Figure 9: Mean trajectories for each clustered trajectory group from three NADP sites across the State of Texas in 2011 with overall cluster contribution in parentheses. Sites are ordered from west to east, left to right. Top left: TX16 – Sonora. Top Right: TX56 – LBJ National Grasslands. Bottom left: TX10 – Attwater Prairie Chicken NWR.**

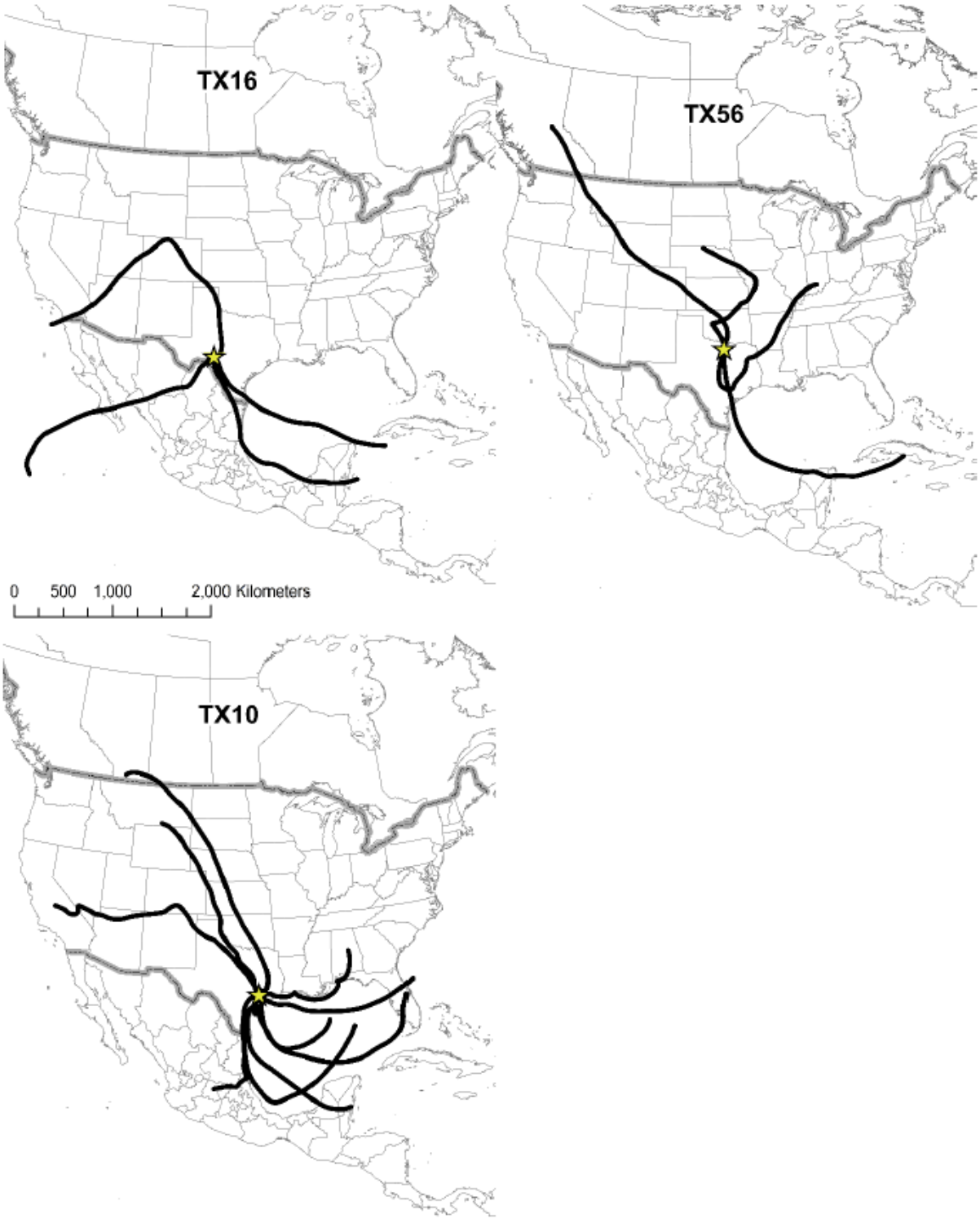


**Figure 10: Trajectory for each individual smoke-influenced rain event (with valid sample collection) occurring at the three focal NADP sites in Texas during 2011. Sites are ordered from west to east, left to right. Top left: TX16 – Sonora. Top Right: TX56 – LBJ National Grasslands. Bottom left: TX10 – Attwater Prairie Chicken NWR.**

Associations among solutes were similar across the three sites. At the Sonora site, four principal components were identified. These components were sea salt, air pollution, dust, and an unknown fourth component. Sea salt and air pollution explained ~87% of the variance (Table 5). At LBJ National Grasslands, four components were identified. These components consisted of air pollution, sea salt, wildfire, and dust. Air pollution and sea salt explained ~74% of the variance, lower than that explained by the first two components at the other sites. The wildfire component explained ~19% of the variance (Table 6). At the Attwater Prairie Chicken NWR location, four components explained ~95% of the variance. Component one was identified as air pollution, component two was identified as sea salt, component three was determined to be wildfire, while component four remains unknown and shows elevated calcium levels which could be indicative of dust. Air pollution and sea salt accounted for 89% of the overall variance, while wildfire accounted for ~3% (Table 7). Overall, a wildfire signature was detectable at Attwater Prairie Chicken NWR and LBJ National Grasslands, the two sites with adequate samples.

**Table 5: Rotated Loadings and Percentage Variance Explained by the First Four Principal Components. Data are for NADP NTN Site TX16, Sonora and for the Year 2011. Bold Indicates Loadings ≥0.74.**

| | Sea Salt | Air Pollution | Dust | Unknown |
|---|---|---|---|---|
| Sodium ($Na^+$) | 0.98 | 0.13 | 0.13 | -0.02 |
| Chloride ($Cl^-$) | 0.96 | 0.23 | 0.00 | 0.05 |
| Magnesium ($Mg^{2+}$) | 0.90 | 0.30 | 0.29 | 0.03 |
| Potassium ($K^+$) | 0.78 | 0.48 | 0.27 | 0.22 |
| Calcium ($Ca^{2+}$) | 0.68 | 0.40 | 0.59 | 0.05 |
| Ammonium ($NH_4^+$) | 0.20 | 0.93 | 0.10 | -0.02 |
| Nitrate ($NO_3^-$) | 0.24 | 0.92 | 0.09 | -0.08 |
| Sulfate ($SO_4^{2-}$) | 0.29 | 0.85 | 0.21 | 0.31 |
| Variance explained | 49.5% | 37.2% | 7.3% | 2.0% |

**Table 6: Rotated Loadings and Percentage Variance Explained by the First Four Principal Components. Data are for NADP NTN Site TX56, LBJ National Grasslands and for the Year in 2011. Bold Indicates Loadings ≥0.74.**

| | Air Pollution | Sea Salt | Wildfire | Dust |
|---|---|---|---|---|
| Nitrate ($NO_3^-$) | 0.94 | 0.11 | 0.16 | 0.23 |
| Ammonium ($NH_4^+$) | 0.84 | 0.34 | 0.39 | -0.06 |
| Sulfate ($SO_4^{2-}$) | 0.82 | 0.39 | 0.30 | 0.10 |
| Calcium ($Ca^{2+}$) | 0.57 | 0.34 | 0.53 | 0.51 |
| Chloride ($Cl^-$) | 0.24 | 0.95 | 0.17 | 0.08 |
| Sodium ($Na^+$) | 0.19 | 0.94 | 0.27 | 0.06 |
| Magnesium ($Mg^{2+}$) | 0.44 | 0.70 | 0.47 | 0.29 |
| Potassium ($K^+$) | 0.42 | 0.43 | 0.79 | 0.11 |
| Variance explained | 38.3% | 35.6% | 18.6% | 5.5% |

**Table 7: Rotated Loadings and Percentage Variance Explained by the First Four Principal Components. Data are for NADP NTN Site TX10, Attwater Prairie Chicken NWR and for the Year in 2011. Bold Indicates Loadings ≥0.74.**

| | Air Pollution | Sea Salt | Wildfire | Unknown |
|---|---|---|---|---|
| Nitrate ($NO_3^-$) | 0.93 | 0.20 | -0.08 | 0.06 |
| Ammonium ($NH_4^+$) | 0.89 | 0.22 | 0.15 | -0.22 |
| Calcium ($Ca^{2+}$) | 0.85 | 0.27 | 0.16 | 0.33 |
| Sulfate ($SO_4^{2-}$) | 0.78 | 0.47 | 0.15 | -0.01 |
| Chloride ($Cl^-$) | 0.19 | 0.98 | 0.06 | -0.01 |
| Sodium ($Na^+$) | 0.20 | 0.98 | 0.00 | 0.01 |
| Magnesium ($Mg^{2+}$) | 0.39 | 0.90 | 0.14 | 0.07 |
| Potassium ($K^+$) | 0.59 | 0.66 | 0.41 | 0.06 |
| Variance explained | 44.7% | 44.2% | 3.4% | 2.1% |

## Discussion

### Historic Drought Drives High Wildfire Activity and Smoke in Texas

During the 2011-2014 historic drought in Texas, 2011 was the year with the most wildfires, the largest wildfires, and the most extensive area burned. In fact, 72% of all wildfires occurred in 2011, burning a total of approximately 1.12 million hectares. Comparatively

speaking, the entire western US (California, Oregon, Washington, Montana, Wyoming, Nevada, Utah, Colorado, Arizona, and New Mexico) collectively had roughly 1.6 million hectares burned in 2011 (Weber and Yadav 2020). More recently, the State of California has seen 799,254 hectares burned in 2018; 104,813 hectares burned in 2019; and 1.7 million hectares burned in 2020 (https://www.fire.ca.gov/incidents/), putting perspective on the magnitude and severity of the 2011 Texas wildfire season.

It is no surprise that 2011 was the peak of the Texas wildfire season, as 2011 was the driest year of the drought in Texas, as well as the driest year in the recorded history of the state (1895–2020). Record low precipitation amounts were recorded in March, April, May, June, July, and August (https://stateimpact.npr.org/texas/tag/drought/). The length of the wildfire season spanned 350 days in 2011, decreasing as the drought receded to a length of 192 days in 2014. Despite the wildfire season nearly halving in duration from the beginning to the end of the drought, seasonal patterns remained consistent from year-to-year, with spring and summer experiencing the majority of wildfires (61-95%). April was the most active month for wildfires during the drought, mirroring the observed trend in a study conducted by Brey et. al (2018), which concluded that from 2007-2014 April was the most fire prone month in the entirety of the Southern Plains region (Texas, Oklahoma, Arkansas, Louisiana).

Across the focal period, we observed variable patterns of burning across the state. West Texas was affected more by wildfires, containing ~53% of all wildfires and ~82% of the extreme wildfires ($95^{th}$ percentile). During 2011-2014, diverse land cover types were ignited by wildfires. Eleven of the twelve Level Three EPA Ecoregions within Texas contained a wildfire. However, despite the diversity in the location of wildfires by ecoregion, the arid ecoregions of West Texas containing large amounts of shrub/scrub and grassland/herbaceous land cover were

disproportionally burned by wildfires. Fourteen of the seventeen largest wildfires had >50% of the land cover burned classified as shrub/scrub, while the remaining three wildfires largely consumed evergreen forest land covers.

Interestingly, despite wildfires being concentrated in West Texas, smoke showed a contrasting pattern. In 2011, the 'big burn' year, NADP sites located in East Texas were affected by two-times more smoke days and about three times more heavy smoke days compared to West Texas. Our results are supported by a recent study that showed similar spatial patterns in smoke across Texas from 2007-2014, with East Texas receiving more smoke days than West Texas (Brey et al. 2018).

West and East Texas also differed in smoke source regions. Western sites largely received smoke from the Rocky Mountain region and Mexico, while East Texas sites were dominated by smoke from the Southern Plains. For example, Big Bend (West Texas) received 57% of its smoke from Mexico and the Rocky Mountains and only 11% of smoke from the Southern Plains, explained by wind directions and location southwest of the Southern Plains, while Attwater Prairie Chicken NWR (East Texas) received 68% of its smoke from the Southern Plains and 11% from Mexico and the Rocky Mountains. Brey et al. (2017) concluded that the main contributors of smoke to the Southern Plains region (Texas, Louisiana, Arkansas, Oklahoma) were from "outside" (non-US) areas, the Southwest, Southern Plains, Rocky Mountains, and the Northwest. No Northwest sourced smoke was found during our study, though it is possible it occurred outside of 2011 or affected other Southern Plains states (Oklahoma, Arkansas, Louisiana). Smoke sources also showed diversity by site, with sites such as Beeville receiving smoke from nine distinct source regions, while others, such as Big Bend, received smoke from only six distinct regions.

Our study showed major impacts of historic drought on wildfire and smoke in the State of Texas. Within the Great Plains, wildfires have increased in frequency and magnitude in recent decades (Donovan et al. 2017) as well as in the Southwest US (Hallar et al. 2017). With indications of increased drought occurrence and megadroughts across much of the Great Plains and Southwest, warmer average temperatures, as well as poor land management and suppression strategies (IPCC 2014; Cook et al. 2015; Donovan et al. 2017; Hallar et al. 2017), we expect impacts of wildfire and smoke within Texas to also increase. When coupled with large amounts of smoke arriving to Texas from other regions, these findings highlight the need for an understanding of how wildfire smoke affects the chemical composition of precipitation and deposition to ecosystems.

## Wildfire Smoke Contributes to Increased Rainwater Nutrient and Pollutant Concentrations and Deposition

At both sites where precipitation was more frequently affected by wildfire smoke (L.B.J. Grasslands and Attwater Prairie in East Texas), smoke-influenced rainwater samples contained higher concentrations of $K^+$ and $NH_4^+$ compared to background samples. At Attwater Prairie Chicken NWF, $K^+$ and $NH_4^+$ concentrations were about twofold higher, whereas at LBJ National Grasslands concentrations were fivefold and threefold higher, respectively, in smoke-influenced rain samples compared to background samples. Potassium concentration in aerosols is widely used as a tracer of biomass burning given the abundance of K in plant tissues, and studies have shown elevated concentrations in rainwater samples as well (Ponette-González et al. 2016; Myers-Pigg et al. 2017). Certain studies (e.g., Pauliquevis et al. 2012) note the enhancement of $NH_4^+$ in aerosol during biomass burning, although they did not find such a relationship within precipitation and overall deposition. Still, another study focusing on tropical forest peat-based wildfires found enhancements in N and P deposition as a result of biomass burning (including

$NH_4^+$ (Ponette-González et al. 2016).

There were some notable differences in the composition of smoke-influenced rain samples between LBJ National Grasslands and Attwater Praire Chicken NWR. At the latter site, $Ca^{2+}$ and $NO_3^-$ concentrations were also higher in smoke-influenced rainfall samples. The crustal element $Ca^{2+}$ is indicative of dust both in aerosols and precipitation (Avila et al. 1998; Pauliquevis et al. 2012; Brahney et al. 2013; Ponette-González et al. 2018) but can also be drawn into the atmosphere through turbulence created during large wildfires (Shlosser et al. 2017). Other studies have shown the prevalence of $NH_3$ and $NO_x$ emissions from wildfires, noting that grasslands (Baker et al. 2019) and tropical forests emit the highest quantities of these aerosols (Cruz-López et al. 2019). In contrast to Attwater Prairie Chicken NWR, LBJ National Grasslands showed a twofold increase in $Mg^{2+}$, and nearly a twofold increase for $Na^+$, $SO_4^{2-}$, and $Cl^-$. Studies show enhancements of multiple ions and elements in aerosols and rainwater following fire and these differences are likely due to diverse factors, including vegetation type, fire type, land use, and anthropogenic sources (Pauliquevis et al. 2012; Mallia et al. 2015; Ponette-González et al. 2016; Donovan et al. 2017).

Smoke-influenced rainfall samples comprised one quarter to one third of all rainfall samples at the Attwater and LBJ sites, yet account for large amounts of deposition for many analytes. At Attwater Prairie Chicken NWR, 28% of all $Ca^{2+}$ deposition, 25% of $NH_4^+$ and $NO_3^-$ deposition, and 20% of $K^+$ deposition were deposited during smoke-affected weeks. These results are supported by Shlosser et al. (2017), who found that wildfire smoke plumes led to a 148% increase in airborne $Ca^{2+}$ presence, a 486% enhancement in $NO_3^-$, and a 438% enhancement in $K^+$ levels for western US wildfires – which, combined with adequate precipitation, would likely result in higher deposition amounts for these ions.

At LBJ National Grasslands, smoke-influenced sample weeks produced 71% of annual $Ca^{2+}$ and $K^{+}$, 62% of annual $Mg^{2+}$ deposition, and between 48-59% of deposition of all other analytes. This was due to an "extreme deposition event" recorded on June 18th, 2011. On this date, a large wildfire ignited in Brooks County in South Texas. Backward trajectories show that air masses arriving at LBJ crossed smoke emitted from this wildfire from ground level up to 1500 m agl for the 18 hours prior to precipitation being recorded. Official reports differ on the size of the wildfire, with the MTBS reporting a value of ~7,800 ha burned, while NOAA reports ~11,700 ha burned (see SMAC Ranch Fire; https://www.ncdc.noaa.gov/stormevents/eventdetails.jsp?id=311704). This would make the wildfire either the 27th or 17th largest during 2011 (234 recorded wildfires burning ≥ 405ha). In addition to high fire emissions, the LBJ NADP location recorded ~102 mm of precipitation during this sample week, ranking as the second largest amount for the year. The combination of a large wildfire and high precipitation led to the disproportionately large deposition amounts recorded for the week and indicates the potential impact of large wildfires on depositional loading.

Wildfire Source Regions Contribute to Heterogeneity in Rainwater Chemistry and Deposition

Overall chemical signatures and air mass sources were similar for the three Texas NADP sites. The two leading components for all three sites consisted of sea salt, and air pollution. At the Attwater Prairie Chicken NWR and LBJ sites, the most important source is air pollution. The dominant component was composed of $NO_3^{-}$, $NH_4^{+}$, and $SO_4^{2-}$ which are indicators of air pollution and fossil fuel combustion (Park et al. 2004; Pan et al. 2016). The air mass trajectories for these locations show a coincidence with major metropolitan areas in Texas, such as DFW, Austin, San Antonio, and Houston. Each of the three sites had a strong sea salt signature and are

strongly influenced by marine air masses. The sea salt prevalence at all three sites can be explained by the prevailing winds which are southerly. At LBJ National Grasslands, the leading components also indicated air pollution and sea salt. Attwater Prairie Chicken NWR and the LBJ sites showed elevated $K^+$ and $Ca^{2+}$, interpreted as a biomass burning signature. We attribute this to the proclivity of wildfires as well as an adequate sample size for these two sites, while Sonora contained a lower sample size and did not register a biomass burning signature.

However, there was variation among source regions for smoke-influenced samples among the sites, and this was reflected in differences in the rainwater chemical composition for the smoke-influenced rainwater samples. At the Attwater site, smoke generally originated in agricultural areas, arid shrub/scrub (or grassland), and a mixture of forested areas. These samples contained elevated levels of $K^+$, $Mg^{2+}$, and $Na^+$. The elevated $Mg^{2+}$ and $Na^+$ can be attributed to the 70% of smoke-influenced trajectories which spent considerable time over the Gulf of Mexico. In contrast, the smoke-influenced trajectories at LBJ National Grasslands indicate air masses were affected by fires in grassland/herbaceous, agricultural land, and tropical evergreen forest. Concentration data for LBJ National Grasslands showed significant increases for $Ca^{2+}$ and $NH_4^+$. Significant $NH_4^+$ increases have been attributed to tropical forest wildfires and could be indicative of the southern Mexico and Central American smoke origins (Pauliquevis et al. 2012; Ponette-González et al. 2016) and/or hot and dry years conditions across the western and southeastern US that promote smoldering conditions and greater associated $NH_3$ emissions (Bray et al. 2016). It is known that $Ca^{2+}$ is stored within grassland leaves and shoots, being emitted into the atmosphere once burned (Bierle 2012). Four smoke-influenced trajectories originated from the Great Plains. It is possible this produced the stronger $Ca^{2+}$ and $K^+$ loadings based on these source regions.

## Conclusions

In conclusion this study examined wildfire and smoke frequency, magnitude, and distribution in Texas during the 2011-2014 drought. Our findings show that the peak of the drought (2011) coincided with the majority of extreme wildfires during the focal period, with the majority of wildfires occurring in shrub/scrub and grassland/herbaceous areas of West Texas. Our findings also indicate that smoke occurrence at Texas NADP sites arrives from a diverse set of regions outside of the Southern Plains. Smoke was shown to be transported from regions such as Canada, Central America, Mexico, the Rocky Mountains, and Southwest. We find that West Texas smoke occurrence was more equally portioned amongst source regions, while East Texas sites received most of their smoke from the Southern Plains region. We note that at two of the three sites (Attwater Prairie Chicken NWR and LBJ National Grasslands), wildfire appeared in the first four principal components in 2011. Lastly, we note enhanced concentrations of multiple analytes within smoke-influenced rainwater samples, as well as significantly increased wet deposition amounts for various analytes, such as $Ca^{2+}$ and $K^{+}$ accounting for 71% of annual deposition in 2011, despite smoke-influenced samples only constituting 22% of the total. Our findings indicate that wildfire plays a significant role in precipitation chemistry as well as deposition. Given projections for the future climate in the Great Plains region, it is imperative to understand potential ecological and human effects of wildfire influenced precipitation events.

# CHAPTER 3

# CONCLUSIONS

## Contributions to the Field of Geography

This study contributes to the field of geography in multiple spatiotemporal aspects. First, we analyzed the spatial and temporal distribution of wildfires across Texas during the 2011-2014 historic drought. Spatially, we discovered that a vast majority of wildfires during this period occurred in West Texas, with East Texas containing the second highest concentration of wildfires. Southern and Central Texas contained few wildfires in comparison. Large wildfires were largely located in West Texas. These findings contribute to the understanding of fire-prone regions across the state. Further, it highlights the susceptibility of shrub/scrub and grassland/herbaceous areas to producing and fueling large wildfires. It is also important to note that these regions are typically located within private land with limited access and difficult topography to navigate, making containment and response more difficult for fast moving wildfires. Temporally, ~72% of all wildfires during the focal period occurred during the peak year of the drought (2011), with spring months, particularly April, containing the most wildfires. Lastly, this study contributes to the knowledge surrounding wildfire and smoke influence across the entirety of Texas while also increasing understanding of precipitation chemistry across three diverse sites within the state.

Overall, this study has direct implications for land use management, policy, and further research. Land managers would benefit from knowing which areas of Texas are most prone to wildfire impacts, which land covers are most susceptible to large wildfires, and what months they might expect increased wildfire activity. Policy makers could use the findings from this study to provide ample funding and support to these land managers during increased risk times,

as well as increasing the ability to respond to wildfires. Further studies could investigate the impacts that deposition of smoke influenced events create on society and the environment. The findings presented in this study have significance in the face of climate change induced future environmental risks, such as increased drought severity and duration, increased temperatures, sporadic and more extreme rainfall events, and thus, the increased risk of wildfires across Texas (Nielsen-Gammon 2011; IPCC 2014; USGCRP 2018).

## Significance of Wildfire and Smoke during the 2011-2014 Texas Drought

This study found numerous significant results pertaining to wildfire and smoke during the historic drought that took place in Texas from 2011-2014. It found that wildfires disproportionately affected West Texas, specifically in 2011 (the peak of the drought). A historically wet 2010 led to a sizeable fuel loading potential across the state (Nielsen-Gammon 2011; McGregor 2015), thus, in 2011, as the drought came to its apex with far above average temperatures and a lack of rainfall, there was an abundance of fuel for wildfires to consume. This historic fire season compared astonishingly well with recent Western US wildfires, consuming 1.12 million hectares within Texas while the entire Western US contained 1.6 million burned hectares in 2011 (Weber & Yadav 2011). Even more so, California contained roughly ~800,000 hectares burned in 2018, ~105,000 hectares in 2019, and ~1.7 million hectares in the record setting 2020 wildfire season (CAL FIRE 2021). Despite the abundance of wildfire in West Texas, East Texas NADP sites were more heavily impacted by smoke presence, containing roughly twofold to threefold more smoke days than those in the western portion of the state. We found smoke impacted each NADP site from at least six distinct regions and as many as nine, highlighting the importance of further research into smoke influenced events, source regions, and local and regional wildfire patterns. We discovered that despite accounting for a relatively small

number of overall samples (<35%), smoke-influenced events accounted for as much as 71% of annual deposition for analytes such as $Ca^{2+}$ and $K^{+}$ and as high as a fivefold increase in concentration for these same analytes, both of which are noted biomass burning markers (Pauliquevis 2012; Ponette-González et al. 2016; Shlosser et al. 2017). These findings highlight the significance of smoke-influenced events to deposition and precipitation chemistry and are points of emphasis for future research into the impacts of amplified drought and wildfire regimes.

## Contributions and Further Research into Smoke-Influenced Events

There have been numerous studies on precipitation chemistry and deposition (da Roacha et al. 2005; Mahowald et al. 2005; Sundarambal et al. 2010; Ponette-González et al. 2016; Ponette-González et al. 2018) as well as numerous studies which have utilized the HMS database, NADP data, and/or HYSPLIT for analysis (Hooper & Peters 1989; McNamara et al. 2000; Brey et al. 2017; Ponette-González et al. 2018). However, these studies have not focused on the impacts of wildfire on precipitation chemistry and environmental deposition (e.g., Ponette-González et al. 2018 focused on dust-in-rain events), nor have they focused on smoke-influenced events in Texas during a drought. This study represents an attempt at filling a portion of the large existing knowledge gap by analyzing the impacts of smoke-influenced precipitation events recorded during the historic 2011-2014 Texas drought utilizing multiple wildfire databases, the NADP, and HYSPLIT. This contribution also provides increased understanding of chemical and depositional impacts of drought and wildfire regimes in the face of climate change within Texas, the Southern Plains, and the Great Plains.

Future research will build upon these findings and seek to explore the relationship between chemical profiles recorded during smoke-influenced events and the type of land cover

and fuel consumed during the wildfire, as this was not a focal point of this study. The accompanying future research will seek to prove a greater spatial and temporal scale by providing analysis for all eight Texas NADP locations during the entirety of the 2011-2014 drought period. Conducting this research will provide a more complete analysis of chemical signatures of smoke-influenced events, as well as a clearer picture of spatial impacts and variations of wildfire and smoke across Texas including accompanying depositional data. This research will ultimately help to provide a glimpse of the potential impacts of future intensifying drought and wildfire regimes in the Southern Plains region.

REFERENCES

American Association of Port Authoritis (AAPA) (2015). *Port Industry Statistics.* Retrieved from https://www.aapa-ports.org/unifying/content.aspx?ItemNumber=21048

Avila, A., Alarcón, M., & Queralt, I. (1998). The chemical composition of dust transported in red rains—Its contribution to the biogeochemical cycle of a holm oak forest in Catalonia (Spain). *Atmospheric Environment*, *32*(2), 179–191. https://doi.org/10.1016/S1352-2310(97)00286-0

Balch, J. K., Bradley, B. A., Abatzoglou, J. T., Nagy, R. C., Fusco, E. J., & Mahood, A. L. (2017). Human-started wildfires expand the fire niche across the United States. *Proceedings of the National Academy of Sciences*, *114*(11), 2946. https://doi.org/10.1073/pnas.1617394114

Beierle, M. J. (2012). *Biophysical and human characteristics of wildfire ignition in the shortgrass prairie region of Texas* [Thesis]. https://ttu-ir.tdl.org/handle/2346/47474

Bodí, M. B., Martin, D. A., Balfour, V. N., Santín, C., Doerr, S. H., Pereira, P., Cerdà, A., & Mataix-Solera, J. (2014). Wildland fire ash: Production, composition and eco-hydro-geomorphic effects. *Earth-Science Reviews*, *130*, 103–127. https://doi.org/10.1016/j.earscirev.2013.12.007

Bond, T. C., Doherty, S. J., Fahey, D. W., Forster, P. M., Berntsen, T., DeAngelo, B. J., Flanner, M. G., Ghan, S., Kärcher, B., Koch, D., Kinne, S., Kondo, Y., Quinn, P. K., Sarofim, M. C., Schultz, M. G., Schulz, M., Venkataraman, C., Zhang, H., Zhang, S., … Zender, C. S. (2013). Bounding the role of black carbon in the climate system: A scientific assessment. *Journal of Geophysical Research: Atmospheres*, *118*(11), 5380–5552. https://doi.org/10.1002/jgrd.50171

Brahney, J., Ballantyne, A. P., Sievers, C., & Neff, J. C. (2013). Increasing Ca2+ deposition in the western US: The role of mineral aerosols. *Aeolian Research*, *10*, 77–87. https://doi.org/10.1016/j.aeolia.2013.04.003

Bray, C., Battye, W., Aneja, V., Tong, D., Lee, P., & Tang, Y. (2016). Impact of Wildfires on Atmospheric Ammonia Concentrations in the US: Coupling Satellite and Ground Based Measurements. *Proceedings of The 1st International Electronic Conference on Atmospheric Sciences*, B001. https://doi.org/10.3390/ecas2016-B001

Bray, C. D., Battye, W., Aneja, V. P., Tong, D. Q., Lee, P., & Tang, Y. (2018). Ammonia emissions from biomass burning in the continental United States. *Atmospheric Environment*, *187*, 50–61. https://doi.org/10.1016/j.atmosenv.2018.05.052

Brey, S. J., Ruminski, M., Atwood, S. A., & Fischer, E. V. (2018). Connecting smoke plumes to sources using Hazard Mapping System (HMS) smoke and fire location data over North America. *Atmos. Chem. Phys.*, *18*(3), 1745–1761. https://doi.org/10.5194/acp-18-1745-2018

Cayan, D. R., Das, T., Pierce, D. W., Barnett, T. P., Tyree, M., & Gershunov, A. (2010). Future dryness in the southwest US and the hydrology of the early 21st century drought. *Proceedings of the National Academy of Sciences*, *107*(50), 21271. https://doi.org/10.1073/pnas.0912391107

Cook, B. I. , Ault, T. R. , & Smerdon, J. E. (2015). Unprecedented 21st century drought risk in the American Southwest and Central Plains. Science Advances, 1(1), e1400082. https://doi.org/10.1126/sciadv.1400082

Dadashazar, H., Ma, L., & Sorooshian, A. (2018). Sources of pollution and interrelationships between aerosol and precipitation chemistry at a central California site. *Science of The Total Environment*, *651*, 1776–1787. https://doi.org/10.1016/j.scitotenv.2018.10.086

Dennison, P. E., Brewer, S. C., Arnold, J. D., and Moritz, M. A. (2014), Large wildfire trends in the western United States, 1984–2011, *Geophys. Res. Lett.*, 41, 2928– 2933, https://doi.org/10.1002/2014GL059576

De Simone, F., Cinnirella, S., Gencarelli, C. N., Yang, X., Hedgecock, I. M., & Pirrone, N. (2015). Model Study of Global Mercury Deposition from Biomass Burning. *Environmental Science & Technology*, *49*(11), 6712–6721. https://doi.org/10.1021/acs.est.5b00969

DeSantis, R. D., Hallgren, S. W., & Stahle, D. W. (2011). Drought and fire suppression lead to rapid forest composition change in a forest-prairie ecotone. *Forest Ecology and Management*, *261*(11), 1833–1840. https://doi.org/10.1016/j.foreco.2011.02.006

Donovan, V. M., Wonkka, C. L., and Twidwell, D. (2017), Surging wildfire activity in a grassland biome, *Geophys. Res. Lett.*, 44, 5986– 5993, https://doi.org/10.1002/2017GL072901

Donovan, V. M., Twidwell, D., Uden, D. R., Tadesse, T., Wardlow, B. D., Bielski, C. H., Jones, M. O., Allred, B. W., Naugle, D. E., & Allen, C. R. (2020). Resilience to Large, "Catastrophic" Wildfires in North America's Grassland Biome. *Earth's Future*, *8*(7), e2020EF001487. https://doi.org/10.1029/2020EF001487

Fraser, A., Dastoor, A., & Ryjkov, A. (2018). How important is biomass burning in Canada to mercury contamination? *Atmospheric Chemistry and Physics*, *18*(10), 7263–7286. https://doi.org/10.5194/acp-18-7263-2018

Friedli, H. R., Arellano, A. F., Cinnirella, S., & Pirrone, N. (2009). Initial Estimates of Mercury Emissions to the Atmosphere from Global Biomass Burning. *Environmental Science & Technology*, *43*(10), 3507–3513. https://doi.org/10.1021/es802703g

Hallar, A. G., Molotch, N. P., Hand, J. L., Livneh, B., McCubbin, I. B., Petersen, R., Michalsky, J., Lowenthal, D., & Kunkel, K. E. (2017). Impacts of increasing aridity and wildfires on aerosol loading in the intermountain Western US. *Environmental Research Letters*, *12*(1), 014006. https://doi.org/10.1088/1748-9326/aa510a

Hoerling, M., Eischeid, J., Kumar, A., Leung, R., Mariotti, A., Mo, K., Schubert, S., & Seager, R. (2013). Causes and Predictability of the 2012 Great Plains Drought. *Bulletin of the American Meteorological Society*, *95*(2), 269–282. https://doi.org/10.1175/BAMS-D-13-00055.1

Hoff, D. L., Will, R. E., Zou, C. B., Weir, J. R., Gregory, M. S., & Lillie, N. D. (2018). Estimating increased fuel loading within the Cross Timbers forest matrix of Oklahoma, USA due to an encroaching conifer, Juniperus virginiana, using leaf-off satellite imagery. *Forest Ecology and Management*, *409*, 215–224. https://doi.org/10.1016/j.foreco.2017.11.003

Hooper, R. P., & Peters, N. E. (1989). Use of multivariate analysis for determining sources of solutes found in wet atmospheric deposition in the United States. *Environmental Science & Technology*, *23*(10), 1263–1268. USGS Publications Warehouse.

Hu, X., Yu, C., Tian, D., Ruminski, M., Robertson, K., Waller, L. A., & Liu, Y. (2016). Comparison of the Hazard Mapping System (HMS) fire product to ground-based fire records in Georgia, USA. *Journal of Geophysical Research: Atmospheres*, *121*(6), 2901–2910. https://doi.org/10.1002/2015JD024448

Intergovernmental Panel on Climate Change (IPCC). (2014). Climate change 2014: Synthesis report: Contribution of Working Groups I, II and III to the fifth assessment report of the Intergovernmental Panel on Climate Change. Retrieved from http://www.ipcc.ch/report/ar5/syr/

Karlsson, P. E., Ferm, M., Tømmervik, H., Hole, L. R., Pihl Karlsson, G., Ruoho-Airola, T., Aas, W., Hellsten, S., Akselsson, C., Mikkelsen, T. N., & Nihlgård, B. (2013). Biomass burning in eastern Europe during spring 2006 caused high deposition of ammonium in northern Fennoscandia. *Environmental Pollution*, *176*, 71–79. https://doi.org/10.1016/j.envpol.2012.12.006

Le Quéré, C., Andrew, R. M., Friedlingstein, P., Sitch, S., Hauck, J., Pongratz, J., Pickers, P. A., Korsbakken, J. I., Peters, G. P., Canadell, J. G., Arneth, A., Arora, V. K., Barbero, L., Bastos, A., Bopp, L., Chevallier, F., Chini, L. P., Ciais, P., Doney, S. C., … Zheng, B. (2018). Global Carbon Budget 2018. *Earth System Science Data*, *10*(4), 2141–2194. https://doi.org/10.5194/essd-10-2141-2018

Lindley, T. T., Speheger, D. A., Day, M. A., Murdoch, G. P., Smith, B. R., Nauslar, N. J., & Daily, D. C. (2019). Megafires on the Southern Great Plains. *Journal of Operational Meteorology*, 164–179. https://doi.org/10.15191/nwajom.2019.0712

Mahowald, N. M., Artaxo, P., Baker, A. R., Jickells, T. D., Okin, G. S., Randerson, J. T., & Townsend, A. R. (2005). Impacts of biomass burning emissions and land use change on Amazonian atmospheric phosphorus cycling and deposition. *Global Biogeochemical Cycles*, *19*(4). https://doi.org/10.1029/2005GB002541

Maidens, A., A. Arribas, A.A. Scaife, C. MacLachlan, D. Peterson, and J. Knight, 2013: The Influence of Surface Forcings on Prediction of the North Atlantic Oscillation Regime of

Winter 2010/11. *Mon. Wea. Rev.,* 141, 3801–3813, https://doi.org/10.1175/MWR-D-13-00033.1

Mallia, D. V., Lin, J. C., Urbanski, S., Ehleringer, J., & Nehrkorn, T. (2015). Impacts of upwind wildfire emissions on CO, CO2, and PM2.5 concentrations in Salt Lake City, Utah. *Journal of Geophysical Research: Atmospheres*, *120*(1), 147–166. https://doi.org/10.1002/2014JD022472

McClure, C. D., & Jaffe, D. A. (2018). US particulate matter air quality improves except in wildfire-prone areas. *Proceedings of the National Academy of Sciences*, *115*(31), 7901. https://doi.org/10.1073/pnas.1804353115

McGregor, K. M. (2015). Comparison of the Recent Drought in Texas to the Drought of Record Using Reanalysis Modeling. *Papers in Applied Geography*, *1*(1), 34–42. https://doi.org/10.1080/23754931.2015.1009295

McNamara, D., Stephens, G., Ruminski, M., & Kasheta, T. (2004). The Hazard Mapping System (HMS)—NOAA'S multi-sensor fire and smoke detection program using environmental satellites. *Conference on Satellite Meteorology and Oceanography*. Retrieved from https://www.researchgate.net/publication/242114643_The_Hazard_Mapping_System_HMS_-_NOAA%27S_multi-sensor_fire_and_smoke_detection_program_using_environmental_satellites

Myers-Pigg, A. N., Griffin, R. J., Louchouarn, P., Norwood, M. J., Sterne, A., & Cevik, B. K. (2016). Signatures of Biomass Burning Aerosols in the Plume of a Saltmarsh Wildfire in South Texas. *Environmental Science & Technology*, *50*(17), 9308–9314. https://doi.org/10.1021/acs.est.6b02132

Nielsen-Gammon, J. W. (2011). The 2011 Texas Drought: A Briefing Packet for the Texas Legislature, October 31, 2011. *OSC Report: The 2011 Texas Drought.*

Nielsen-Gammon, J. W., Banner, J. L., Cook, B. I., Tremaine, D. M., Wong, C. I., Mace, R. E., Gao, H., Yang, Z.-L., Gonzalez, M. F., Hoffpauir, R., Gooch, T., & Kloesel, K. (2020). Unprecedented Drought Challenges for Texas Water Resources in a Changing Climate: What Do Researchers and Stakeholders Need to Know? *Earth's Future*, *8*(8), e2020EF001552. https://doi.org/10.1029/2020EF001552

Olivier, J. G. J., Aardenne, J. A. V., Dentener, F. J., Pagliari, V., Ganzeveld, L. N., & Peters, J. A. H. W. (2005). Recent trends in global greenhouse gas emissions:regional trends 1970–2000 and spatial distributionof key sources in 2000. *Environmental Sciences*, *2*(2–3), 81–99. https://doi.org/10.1080/15693430500400345

Pan, Y., Tian, S., Liu, D., Fang, Y., Zhu, X., Zhang, Q., Zheng, B., Michalski, G., & Wang, Y. (2016). Fossil Fuel Combustion-Related Emissions Dominate Atmospheric Ammonia Sources during Severe Haze Episodes: Evidence from 15N-Stable Isotope in Size-Resolved Aerosol Ammonium. *Environmental Science & Technology*, *50*(15), 8049–8056. https://doi.org/10.1021/acs.est.6b00634

Park, R. J., Jacob, D. J., Field, B. D., Yantosca, R. M., & Chin, M. (2004). Natural and transboundary pollution influences on sulfate-nitrate-ammonium aerosols in the United States: Implications for policy. *Journal of Geophysical Research: Atmospheres*, *109*(D15). https://doi.org/10.1029/2003JD004473

Pasos, M. (2015). Land Cover 30m, 2015 (Landsat and RapidEye). *Commission for Environmental Cooperation*. Retrieved May 31, 2021, from http://www.cec.org/north-american-environmental-atlas/land-cover-30m-2015-landsat-and-rapideye/

Paugam, R., Wooster, M., Freitas, S., & Val Martin, M. (2016). A review of approaches to estimate wildfire plume injection height within large-scale atmospheric chemical transport models. *Atmospheric Chemistry and Physics*, *16*(2), 907–925. https://doi.org/10.5194/acp-16-907-2016

Pauliquevis, T., Lara, L. L., Antunes, M. L., & Artaxo, P. (2012). Aerosol and precipitation chemistry measurements in a remote site in Central Amazonia: The role of biogenic contribution. *Atmos. Chem. Phys.*, *12*(11), 4987–5015. https://doi.org/10.5194/acp-12-4987-2012

Ponette-González, A. G., Curran, L. M., Pittman, A. M., Carlson, K. M., Steele, B. G., Ratnasari, D., Weathers, K. C. (2016). Biomass burning drives atmospheric nutrient redistribution within forested peatlands in Borneo. *Environmental Research Letters*, *11*(8), 085003. https://doi.org/10.1088/1748-9326/11/8/085003

Ponette-González, A. G., Collins, J. D., Manuel, J. E., Byers, T. A., Glass, G. A., Weathers, K. C., & Gill, T. E. (2018). Wet Dust Deposition Across Texas During the 2012 Drought: An Overlooked Pathway for Elemental Flux to Ecosystems. *Journal of Geophysical Research: Atmospheres*, *123*(15), 8238–8254. https://doi.org/10.1029/2018JD028806

Prein, A., Rasmussen, R., Ikeda, K. *et al.* The future intensification of hourly precipitation extremes. *Nature Clim Change* **7,** 48–52 (2017). https://doi.org/10.1038/nclimate3168

da Rocha, G. O., Allen, A. G., & Cardoso, A. A. (2005). Influence of Agricultural Biomass Burning on Aerosol Size Distribution and Dry Deposition in Southeastern Brazil. *Environmental Science & Technology*, *39*(14), 5293–5301. https://doi.org/10.1021/es048007u

Salguero, J., Li, J., Link to external site, this link will open in a new window, Farahmand, A., & Reager, J. T. (2020). Wildfire Trend Analysis over the Contiguous United States Using Remote Sensing Observations. *Remote Sensing*, *12*(16), 2565. https://doi.org/10.3390/rs12162565

Seager, R., L. Goddard, J. Nakamura, N. Henderson, and D.E. Lee, 2014: Dynamical Causes of the 2010/11 Texas–Northern Mexico Drought. *J. Hydrometeor.,* 15, 39–68, https://doi.org/10.1175/JHM-D-13-024.1

Schlesinger, W. H., Gray, J. T., & Gilliam, F. S. (1982). Atmospheric deposition processes and their importance as sources of nutrients in a chaparral ecosystem of southern California. *Water Resources Research*, *18*(3), 623–629. https://doi.org/10.1029/WR018i003p00623

Schlosser, J. S., Braun, R. A., Bradley, T., Dadashazar, H., MacDonald, A. B., Aldhaif, A. A., Aghdam, M. A., Mardi, A. H., Xian, P., & Sorooshian, A. (2017). Analysis of aerosol composition data for western United States wildfires between 2005 and 2015: Dust emissions, chloride depletion, and most enhanced aerosol constituents. *Journal of Geophysical Research: Atmospheres*, *122*(16), 8951–8966. https://doi.org/10.1002/2017JD026547

Shaw, J. D., Goeking, S. A., Menlove, J., & Werstak, C. E., Jr. (2017). Assessment of Fire Effects Based on Forest Inventory and Analysis Data and a Long-Term Fire Mapping Data Set. *Journal of Forestry*, *115*(4), 258–269. Earth, Atmospheric & Aquatic Science Database; Research Library; SciTech Premium Collection. https://doi.org/10.5849/jof.20l6-115

Shi, Y., Zang, S., Matsunaga, T., & Yamaguchi, Y. (2020). A multi-year and high-resolution inventory of biomass burning emissions in tropical continents from 2001–2017 based on satellite observations. *Journal of Cleaner Production*, *270*, 122511. https://doi.org/10.1016/j.jclepro.2020.122511

Stohl, A., Berg, T., Burkhart, J. F., Fjæraa, A. M., Forster, C., Herber, A., Hov, Ø., Lunder, C., McMillan, W. W., Oltmans, S., Shiobara, M., Simpson, D., Solberg, S., Stebel, K., Ström, J., Tørseth, K., Treffeisen, R., Virkkunen, K., & Yttri, K. E. (2006). *Arctic smoke – record high air pollution levels in the European Arctic due to agricultural fires in Eastern Europe* [Preprint]. https://doi.org/10.5194/acpd-6-9655-2006

Sundarambal, P., Balasubramanian, R., Tkalich, P., & He, J. (2010). Impact of biomass burning on ocean water quality in Southeast Asia through atmospheric deposition: Field observations. *Atmospheric Chemistry and Physics*, *10*(23), 11323–11336. https://doi.org/10.5194/acp-10-11323-2010

Tian, H., Lu, C., Ciais, P., Michalak, A. M., Canadell, J. G., Saikawa, E., Huntzinger, D. N., Gurney, K. R., Sitch, S., Zhang, B., Yang, J., Bousquet, P., Bruhwiler, L., Chen, G., Dlugokencky, E., Friedlingstein, P., Melillo, J., Pan, S., Poulter, B., … Wofsy, S. C. (2016). The terrestrial biosphere as a net source of greenhouse gases to the atmosphere. *Nature*, *531*(7593), 225-228D. https://doi.org/10.1038/nature16946

United States Census Bureau (USCB) (2019). *Metropolitican and Micropolitan Statistical Areas Population Totals and Components of Change: 2010-2015*. Retrieved from https://www.census.gov/data/tables/time-series/demo/popest/2010s-total-metro-and-micro-statistical-areas.html

United States Geological Survey (USGS) (2016). *Land Cover for the Conterminous U.S. Shown as 16 Thematic Classes*. Retrieved from https://www.usgs.gov/media/images/land-cover-conterminous-us-shown-16-thematic-classes

United States Global Climate Research Program (USGCRP). (2018). *Climate Science Special Report: Fourth National Climate Assessment, Volume I* (p. 470). U.S. Global Change Research Program. https://doi.org/10.7930/J0J964J6

Urbanski, S. P., Hao, W. M., & Baker, S. (2008). Chapter 4 Chemical Composition of Wildland Fire Emissions. In A. Bytnerowicz, M. J. Arbaugh, A. R. Riebau, & C. Andersen (Eds.), *Developments in Environmental Science* (Vol. 8, pp. 79–107). Elsevier. https://doi.org/10.1016/S1474-8177(08)00004-1

Wang, S. S.-C., & Wang, Y. (2020). Quantifying the effects of environmental factors on wildfire burned area in the south central US using integrated machine learning techniques. *Atmospheric Chemistry and Physics*, *20*(18), 11065–11087. https://doi.org/10.5194/acp-20-11065-2020

Weber, K. T., & Yadav, R. (2020). Spatiotemporal Trends in Wildfires across the Western United States (1950–2019). *Remote Sensing*, *12*(18), 2959. https://doi.org/10.3390/rs12182959

Webster, J. P., Kane, T. J., Obrist, D., Ryan, J. N., & Aiken, G. R. (2016). Estimating mercury emissions resulting from wildfire in forests of the Western United States. *Science of The Total Environment*, *568*, 578–586. https://doi.org/10.1016/j.scitotenv.2016.01.166

Westerling, A. L. (2016). Increasing western US forest wildfire activity: Sensitivity to changes in the timing of spring. *Philosophical Transactions of the Royal Society B: Biological Sciences*, *371*(1696), 20150178. https://doi.org/10.1098/rstb.2015.0178

Whitburn, S., Van Damme, M., Kaiser, J. W., van der Werf, G. R., Turquety, S., Hurtmans, D., Clarisse, L., Clerbaux, C., & Coheur, P.-F. (2015). Ammonia emissions in tropical biomass burning regions: Comparison between satellite-derived emissions and bottom-up fire inventories. *Atmospheric Environment*, *121*, 42–54. https://doi.org/10.1016/j.atmosenv.2015.03.015

Whittier, T. R., & Gray, A. N. (2016). Tree mortality based fire severity classification for forest inventories: A Pacific Northwest national forests example. *Special Section: Forests, Roots and Soil Carbon*, *359*, 199–209. https://doi.org/10.1016/j.foreco.2015.10.015

Williams, A., Cook, E., Smerdon, J., Cook, B., Abatzoglou, J., Bolles, K., Baek, S. H., Badger, A., & Livneh, B. (2020). Large contribution from anthropogenic warming to an emerging North American megadrought. *Science*, *368*, 314–318. https://doi.org/10.1126/science.aaz9600

Zhao, F., Keane, R., Zhu, Z., & Huang, C. (2015). Comparing historical and current wildfire regimes in the Northern Rocky Mountains using a landscape succession model. *Forest Ecology and Management*, *343*, 9–21. https://doi.org/10.1016/j.foreco.2015.01.020